



**HAL**  
open science

## The Motor Protein Myosin-X Transports VE-Cadherin along Filopodia To Allow the Formation of Early Endothelial Cell-Cell Contacts

Sébastien Almagro, Claire Durmort, Adeline Chervin-Pétinot, Stéphanie Heyraud, Mathilde Dubois, Olivier Lambert, Camille Maillefaud, Elizabeth Hewat, Jean Patrick Schaal, Philippe Huber, et al.

### ► To cite this version:

Sébastien Almagro, Claire Durmort, Adeline Chervin-Pétinot, Stéphanie Heyraud, Mathilde Dubois, et al.. The Motor Protein Myosin-X Transports VE-Cadherin along Filopodia To Allow the Formation of Early Endothelial Cell-Cell Contacts: MYOSIN-X TRANSPORT OF VE-CADHERIN ALONG FILOPODIA. *Molecular and Cellular Biology*, 2010, Apr. 2010, page 1703-1717. 10.1128/MCB.01226-09 . inserm-00462307

**HAL Id: inserm-00462307**

**<https://inserm.hal.science/inserm-00462307>**

Submitted on 9 Mar 2010

**HAL** is a multi-disciplinary open access archive for the deposit and dissemination of scientific research documents, whether they are published or not. The documents may come from teaching and research institutions in France or abroad, or from public or private research centers.

L'archive ouverte pluridisciplinaire **HAL**, est destinée au dépôt et à la diffusion de documents scientifiques de niveau recherche, publiés ou non, émanant des établissements d'enseignement et de recherche français ou étrangers, des laboratoires publics ou privés.

# The motor protein Myosin-X transports VE-cadherin along filopodia to allow the formation of early endothelial cell-cell contacts

Sébastien Almagro,<sup>1,2,3</sup> Claire Durmort,<sup>3,4</sup> Adeline Chervin-Pétiot,<sup>1,2,3</sup> Stephanie Heyraud,<sup>1,2,3,4</sup> Mathilde Dubois,<sup>6</sup> Olivier Lambert,<sup>6</sup> Camille Maillefaud,<sup>3,4</sup> Elizabeth Hewat,<sup>5</sup> Jean Patrick Schaal<sup>7</sup>, Philippe Huber<sup>1,2,3</sup> and Danielle Gulino-Debrac<sup>1,2,3\*</sup>

Laboratoire de Physiopathologie Vasculaire, CEA, 38054 Grenoble, France,<sup>1</sup> INSERM U882, 38054 Grenoble, France,<sup>2</sup> Université Joseph Fourier, Grenoble, France,<sup>3</sup> Laboratoire d'Ingénierie des Macromolécules,<sup>4</sup> Laboratoire de Microscopie Electronique Structurale, Institut de Biologie Structurale Jean-Pierre Ebel UMR CNRS 5075, Grenoble, France,<sup>5</sup> CBMN UMR CNRS 5248-Institut Européen de Chimie et de Biologie, Université Bordeaux 1, Talence, France,<sup>6</sup> Département de Gynécologie Obstétrique, Centre Hospitalier Universitaire Michallon, Grenoble, France<sup>7</sup>

\* Corresponding author. Mailing address: iRTSV, APV, INSERM U882, CEA-Grenoble, 17 rue des Martyrs, 38054 Grenoble Cedex 9, France. Phone: 33 4 38 78 92 72. Fax: 33 4 38 78 49 64, E-mail: [danielle.gulino@cea.fr](mailto:danielle.gulino@cea.fr)

**Vascular endothelium, the monolayer of endothelial cells that lines the vascular tree, undergoes damages at the basis of some vascular diseases. Its integrity is maintained by VE-cadherin, an adhesive receptor localized at cell-cell junctions. Here, we show that VE-cadherin is also located at the tip and along filopodia in sparse or subconfluent endothelial cells. We observed that VE-cadherin navigates along intrafilopodial actin filaments. We found that the actin motor protein myosin-X is co-localized and moves synchronously with filopodial VE-cadherin. Immunoprecipitation and pull-down assays confirmed that myosin-X is directly associated with the VE-cadherin complex. Furthermore, expression of a dominant-negative mutant of myosin-X revealed that myosin-X is required for VE-cadherin export to cell edges and filopodia. These features indicate that myosin-X establishes a link between the actin cytoskeleton and VE-cadherin, thereby allowing VE-cadherin transportation along intrafilopodial actin cables. In conclusion, we propose that VE-cadherin trafficking along filopodia using myosin-X motor protein is a pre-requisite for cell-cell junction formation. This mechanism may have functional consequences for endothelium repair in pathological settings.**

The endothelium is composed of a monolayer of endothelial cells that lines the vascular tree. Hemodynamic forces, immune-mediated mechanisms or drug ingestion can injure the endothelium (35). These damages are frequently accompanied by a loss of endothelium integrity, an increase in vascular permeability and possibly by a detachment of endothelial cells from vascular walls (14). These alterations can be circumvented by initiating rapid repair mechanisms that re-establish endothelium integrity and consequently reduce the extent of vascular diseases. The molecular mechanisms at the basis of the endothelium repair process remain elusive but it can be assumed that the reconstitution of

endothelium integrity requires cell-cell junction rebuilding.

In the endothelium, intercellular adherence is maintained by tight and adherens junctions. Adherens junctions are particularly crucial in controlling the formation and maintenance of interendothelial adhesion and constitute dynamic structures that undergo remodelling in migrating as well as resting cells (31). They are essentially composed of vascular endothelial-cadherin (VE-Cad) (22), an adhesive receptor able to elaborate homophilic / homotypic interactions via its extracellular domain and to recruit, through its cytoplasmic tail, partners such as catenins ( $\alpha$ ,  $\beta$ ,  $\gamma$  and p120). Catenins, in turn, promote the

association of the adherens junction with the actin cytoskeleton, another player regulating vascular endothelial barrier function, by molecular mechanisms that are incompletely defined (8). Although there is a general agreement about the critical role played by actin filaments in the maintenance of mature cell-cell junctions (41;27), their precise role in the elaboration of premature adherens junctions is poorly understood. Some studies indicate that cells form intercellular junctions by a dynamic process driven by actin polymerization (38). It was proposed but, in our knowledge not firmly demonstrated, that cell-cell junction formation is initiated by the production of filopodia emanating from neighbouring cells (3; 30; 39; 42). Filopodia lead to the elaboration of puncta which correspond to micro-domains where cadherin molecules concentrate together with their intracellular partners (3). These puncta spatially coincide with cell membrane attachment sites for actin filaments (2). The mechanism by which puncta are elaborated remains to be elucidated.

Filopodia are highly dynamic structures filled with bundles of linear actin filaments (15). Their protrusions is driven by actin polymerization taking place at filament barbed ends that are mainly located at filopodium tips (24). The precise mechanisms of the nucleation and elongation of filopodia are controversial. In fact, two mechanisms for their formation have been proposed, each using different sets of actin-regulating proteins. According to the “convergent elongation model”, filopodia are continuously initiated by the elongation of pre-existing lamellipodial actin filaments (34). This remodelling of actin filaments should require the branching activity of Arp2/3 (29), the F-actin-bundling activity of fascin along filopodium shafts and the anti-capping activity of Ena/VASP at the barbed ends of actin filaments (4). In the opposing model, it was proposed that some members of the formin family such as Dia2 perform all these activities (17). Indeed, *in vitro*, Dia2 nucleates linear actin filaments, accelerates actin polymerization, protects barbed ends from capping proteins thus slowing actin depolymerization (17; 7). Additionally, new players such as Myosin-X (MyoX), able to induce filopodium formation have been recently discovered.

Here, using cryo-electron microscopy, we show that VE-cadherin is not exclusively located at cell-cell junctions but is also present along and at the tip of filopodia in sparse endothelial cells. By videomicroscopy, we observed that VE-cadherin migrates along filopodia in forward and backward

movements. We hypothesized that motor proteins of the myosin family may be involved in the VE-cadherin transportation along filopodia. We considered MyoX as a potential candidate for promoting VE-cadherin trafficking.

Myosins participate in a range of diverse cellular processes such as cell migration, membrane trafficking and formation of cellular protrusions. They share conserved structural features such as a motor domain located at their N-termini that can bind to actin filaments and hydrolyze ATP to produce movement and force. At their C-termini, members of the unconventional myosin family such as myosin-VII, -X, -XII and -XV exhibit a myosin tail homology 4 domain (MyTH4) followed by a band 4.1 Ezrin, Radixin, Moesin (FERM) domain that confer them with the ability to perform unique cellular functions (6). A fascinating feature of MyoX is to use its motor activity to move along the intrafilopodial actin filaments. This probably allows MyoX to carry cargos along filopodia. Potential cargos are the  $\beta$ -chains of integrins recently reported to directly interact with the FERM domain of MyoX (43) and Mena/VASP that is synchronously transported with MyoX towards the tip or the base of filopodia (36). In addition to its motor and transport functions, MyoX also promotes the formation of filopodia (5; 9; 37). Hence, MyoX overexpression stimulates filopodium growth (5) whereas its knockdown decreases the filopodium formation (37; 9; 28).

Herein, we discovered that MyoX is colocalized with VE-cadherin in filopodia and moves synchronously with it. Using immunoprecipitation experiments and pull-down assays, we demonstrated that MyoX interacts with the VE-Cad-catenin complex. Our data thus support a role of MyoX in the transportation of VE-cadherin along intrafilopodial actin. The forward MyoX-mediated transport facilitates the accumulation of VE-Cad at the tips of filopodia where VE-Cad can interact with partners of adjacent cells thus establishing preliminary cell-cell contacts. Formation of these early cell-cell contacts can be inhibited by blocking MyoX-transport capacity. At filopodium tips, VE-Cad linked to MyoX, but not engaged in homophilic interactions, may also be transported backwards to the cell body by the actin retrograde flow. Once at the lamellipodium

edge, VE-Cad can be picked up again by newly formed filopodia. Our data suggest that MyoX-mediated transport of the VE-Cad-catenin complex along filopodia is a key event required for the early

steps of formation of cell-cell contacts, a process that may be of functional importance in endothelium repair and angiogenesis.

## MATERIALS AND METHODS

### Drugs and antibodies

Fibronectin, latrunculin B, FITC- or rhodamine-phalloidin and mAb against  $\alpha$  catenin and  $\beta$  actin were from Sigma-Aldrich. The mAb antibodies against  $\beta$ ,  $\gamma$  catenins and p120 were from Transduction Laboratories. The affinity-purified pAb against human MyoX from SDI (Newark, DE, USA) was used in Western blot, immunoprecipitation and immunofluorescence analyses. Its biochemical characterization is presented in **Fig 1**. The pAb anti- $\beta$ 1 integrin antibody was a generous gift from C. Albigès-Rizo (**25**) while the pAb antibody anti-GST was from GE Healthcare. The pAb antibody anti-Cad3 was used to immunoprecipitate the VE-Cad-based complex (**18**); (**19**). The anti-VE-Cad antibodies pAb C-19 (Santa Cruz Biotechnology) and mAb BV9 (**11**) (Abcam) were used in Western blot experiments. The monoclonal antibody (mAb) BV9 is directed against the extracellular domain and the polyclonal antibody (pAb) C-19 against the 19 amino acid-peptide at VE-Cad C-terminus. The secondary Cy2- or Cy3-conjugated antibodies were from Jackson ImmunoResearch Laboratories, the Cy5- conjugated antibodies from GE Healthcare and Alexa -488, -555, -633 were purchased from Invitrogen.

### Cell culture

HUVECs were isolated and cultured as previously described (**16**). Only cells on passage 2 were used. HeLa cells and CHO cells were respectively cultured in DMEM (Invitrogen) or in  $\alpha$ -MEM (Invitrogen) supplemented with 10% FCS and antibiotics.

### cDNA constructs and protein expression in *E. coli*

A cDNA fragment containing the sequence encoding the FERM domain of bovine MyoX (K1767-V2051) (**6**) was produced by polymerase chain reaction (PCR) using the two following oligonucleotides: forward: 5'-GTGGATCCAAGTTTGAAAAGCTGGCCGCC-3' and reverse: 5'-TCGACCCGGGTACACGGAGCGCGAGGTGCTGTA -3'. After digestion with BamHI and XmaI, the PCR fragment was then inserted into the pGEX-4T1 (GE Healthcare) to elaborate the vector pGEX-4T1-FERM coding for the FERM domain of MyoX fused with an N-terminus GST (GST-FERM). The protein GST-FERM was then produced in BL21-RIL (Stratagene) and purified from inclusion bodies dissolved in urea. The protein was *in vitro* refolded by rapid dilution in 50 mM Tris/HCl, pH 8 buffer containing 150 mM NaCl prior to be captured on a glutathione-Sepharose column. The 59 kDa recombinant protein was purified to homogeneity after elution using reduced glutathione. The His-tagged cytoplasmic domain of VE-Cad was obtained as previously described (**40**).

### Eukaryotic expression vectors

The vector encoding GFP-MyoX was kindly provided R. Cheney (**1**). Pro-VE-Cad cDNA was sub-cloned in the Clontech vectors pAmCyan1-N1, pZsYellow1-N1 to express VE-Cad C-terminally fused with CFP (VE-CFP) and YFP (VE-YFP). Additionally, Pro-VE-Cad was also C-terminally fused with the tdimer 2 of DsRed using the vector pcDNA3.1-DsRed previously described (**12**). This protein,

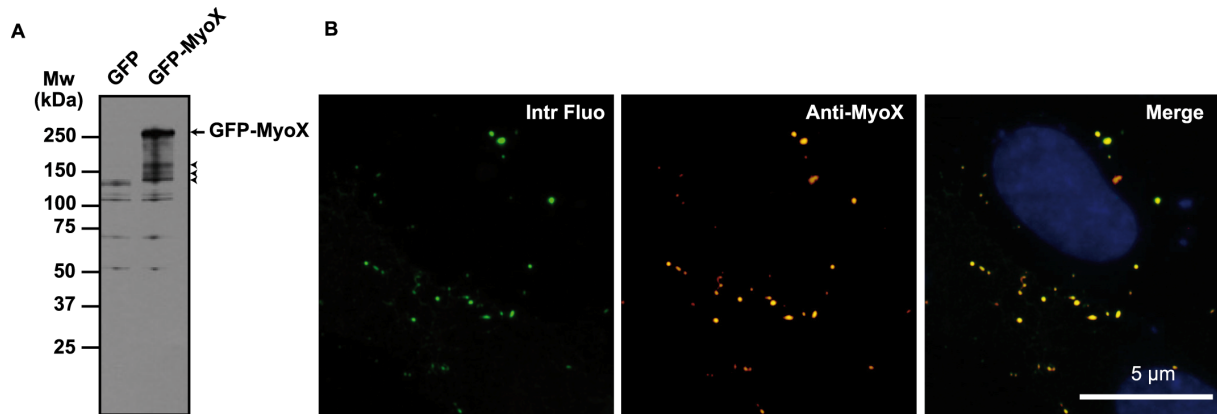


FIG. 1. Biochemical characterization of the anti-MyoX antibody. (A) The rabbit polyclonal Anti-Myosin-X antibody identified a polypeptide band of expected molecular mass in lysates of GFP-MyoX-expressing CHO cells. By contrast, no specific band was detected in lysates of GFP-expressing CHO cells indicating that no MyoX is expressed in CHO cells. The arrow points out intact GFP-MyoX whereas arrow heads indicate degradation products. (B) CHO cells expressing GFP-MyoX were immunofluorescently stained for MyoX. We observed that the intrinsic fluorescence of the GFP tag (Intr fluo) co-localized with the immunostaining of MyoX (Anti- MyoX) thus attesting the specificity of the antibody for MyoX.

designated as VE-DSR, remained monomeric because of its fusion with a tandem dimer of DsRed. Indeed, formation of intramolecular contacts between the tandem DsRed moieties within the same polypeptide prevents protein oligomerization (12). Additionally, the tandem DsRed motif rendered VE-DSR resistant to photobleaching and consequently perfectly well-adapted to videomicroscopy experiments. The characterization of these fluorescent proteins is presented in Fig 2. The specificity of VE-DSR and GFP-MyoX localization in double-fluorescently transfected HUVECs was also controlled (Fig 3). To express in HUVECs and CHO cells the protein GST-FERM-DSR, the eukaryotic expression vector pcDNA3.1-GST-FERM-DSR was constructed by amplifying by PCR the cDNA coding for the GST-FERM protein. This was performed using the *E. coli* expression vector pGEX-4T1-FERM and the primers 5'-CACATCTAGAATGTCCCCTATACTAGGTTAT 3' and 5'-GCAGATATCACGGAGCGCGAGGT -3'. Following digestion by XbaI and EcoRV, this PCR fragment was then introduced in the vector pcDNA 3.1- DSRred to generate the eukaryotic expression vector pcDNA-GST-FERM-DSR coding for GST-FERM-DSR. Similarly, to express in HUVECs and CHO cells, the protein GST-DSR, the eukaryotic expression vector pcDNA-GST-DSR was elaborated by amplifying the cDNA coding for GST. This was made using the

vector pGEX-4T1 (GE-Healthcare) and the primers 5'-CCGCTCGAGATGTCCCCTATACTAGGTTAT 3' and 5'-GCGGATCCTTATCCGATTTTGGAGGATGGT C-3'. Following digestion by XhoI and BamHI, this fragment was inserted into the eukaryotic expression vector pcDNA- DSRred to generate the vector pcDNA-GST-DSR coding for GST-DSR.

#### Transfections

Once seeded on glass coverslips or Labtek I (Nunc, Rochester, NY), HUVECs were transiently transfected using 200 nM polyethylenimine (PEI, Sigma-Aldrich) added in cell medium culture devoid of serum during 45 min at 37°C. HeLa and CHO cells were transfected using Exgen 500 (Euromedex) according to manufacturer protocol.

#### Immunoprecipitation and GST pull-down assays

For pull-down assays, cell lysates (57 cm<sup>2</sup>) were incubated overnight at 4°C with 200 µl of glutathione-beads coupled to either GST or GST-FERM proteins in the presence or absence of 100 µM LaB. After three washing steps in lysis buffer (10 mM PIPES, pH 7.7 containing 100 mM NaCl, 300 mM sucrose, 3 mM MgCl<sub>2</sub>, 1 mM EDTA, 0.5 % NP40), pulled-down proteins were eluted with 100 µl washing buffer containing 20 mM reduced glutathione and then boiled with Laemmli buffer containing β-mercaptoethanol.

For immunoprecipitations, endothelial cell or CHO monolayers (57 cm<sup>2</sup>) were lysed 5 min at 4°C and scrapped in 500 µl RIPA buffer (PBS pH

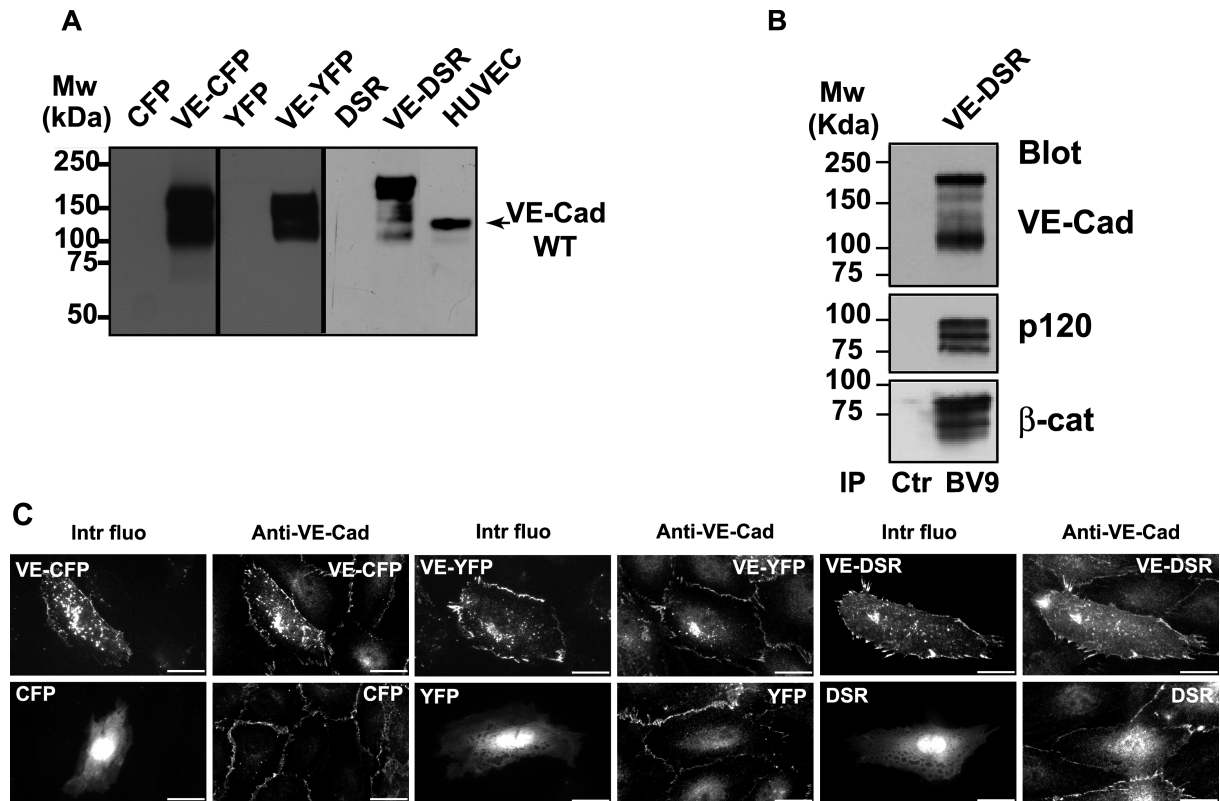


FIG. 2. Characterization of the fluorescent proteins VE-CFP, VE-YFP and VE-DSR. (A) Biochemical characterization of VE-CFP, VE-YFP and VE-DSR. cDNA constructs expressing CFP, VE-CFP, YFP, VE-YFP, DSR and VE-DSR were transfected in CHO cells. At 24 h post transfection, lysates of these transfected cells were analysed by Western blot. The anti-VE-Cad mAb BV9 antibody identified polypeptide bands of 165, 150 and 190 kDa corresponding to the expected sizes for VE-CFP, VE-YFP and VE-DSR respectively. These bands were not detected in lysates of CHO cells expressing CFP, YFP and DSR. In HUVECs used as a control, the wild type form of VE-Cad was detected as a 135 kDa polypeptide band. (B) Co-immunoprecipitation of VE-DSR with catenins. Anti-VE-Cad (IP BV9) immunoprecipitation was performed on VE-DSR-expressing CHO cells prior to be resolved on a 4-12% gradient gel, electro-transferred and probed successively for VE-Cad, p120 and  $\beta$ -cat. As control, an immunoprecipitation performed on VE-DSR-expressing CHO cells using rabbit non-immune IgG (Ctr) was analyzed in parallel. Molecular weight markers are given at the margin of the panel. (C) Localization at cell-cell contacts of exogenous VE-CFP, VE-YFP and VE-DSR transiently expressed in HUVECs. HUVECs expressing VE-CFP, CFP, VE-YFP, YFP, VE-DSR and DSR were immunofluorescently stained for VE-Cad and observed by confocal microscopy. Then, the intrinsic fluorescence of the CFP, YFP and DSR tags (Intr fluo) was compared to the immunofluorescent staining (Anti-VE-Cad). As expected, the three fluorescent VE-Cad proteins were mainly expressed at cell-cell junctions and on filopodia recapitulating the staining pattern of endogenous VE-Cad. By contrast, the proteins CFP, YFP and DSR did not present a specific localization. Bars = 20  $\mu$ m.

7.4, 150 mM NaCl, 1 mM MgCl<sub>2</sub>, 0.5 % Deoxycholate, 1% Triton-X100, 0.1% SDS, 1 mM ATP, containing a protease inhibitor cocktail). Prior pre-clearing, cell lysates were treated with latrunculin B as mentioned for pulled-down experiments. Pre-cleared lysates were immunoprecipitated with the polyclonal anti-MyoX (4  $\mu$ g) or anti-VE-Cad (4  $\mu$ g) antibodies coupled to 1.6 mg of protein-A sepharose (Sigma). Immune complexes were washed three times with RIPA buffer prior to be eluted with 2X Laemmli

buffer 10 min at 100°C and reduced with  $\beta$ -mercaptoethanol.

#### SDS-PAGE and Western blot analysis

MyoX immunoprecipitations were separated by electrophoresis in MOPS buffer (Biorad) on pre-cast Criterion XT 4-12 % gradient Bis-Tris gels (BioRad). The gels were transferred 1h (300 mA) to Immobilon membrane (Millipore) using a Tris-glycine buffer. Then, membranes were blocked with 5% non-fat dry milk and proteins from total cell extracts, immunoprecipitates or pull-down assays were detected by specific primary

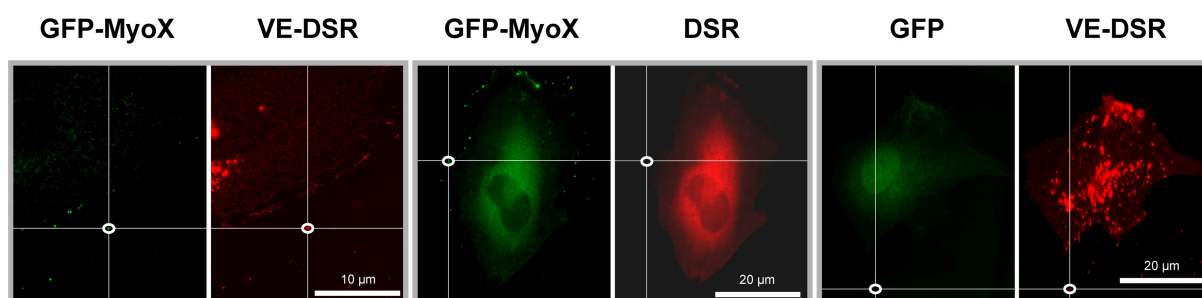


FIG. 3. Specificity of localization of VE-DSR and GFP-MyoX in double-fluorescently transfected HUVECs. To control the specificity of GFP-MyoX localization, HUVECs co-expressing either GFP-MyoX and VE-DSR (panels at left) or GFP-MyoX and DSR (middle panels) were analyzed in green and red fluorescence channels. Using ImageJ, the fluorescent intensity ( $I$ ) of GFP-MyoX spots (delimited by ellipses) were measured and compared to the fluorescent intensities of the superimposed areas in the other channel. While the mean value for  $I_{\text{GFP-MyoX}} / I_{\text{VE-DSR}}$  ratio is ranging 1 (20 measurements from 5 images), that of  $I_{\text{GFP-MyoX}} / I_{\text{DSR}}$  ratio varied between  $3.10^5$  – infinite (20 measurements from 5 images). Similarly, to control the specificity of VE-DSR localization, HUVECs co-expressing GFP and VE-DSR were analyzed in parallel for fluorescent localization (panels at right). While the mean value for  $I_{\text{VE-DSR}} / I_{\text{GFP-MyoX}}$  ratio is ranging 1, that of  $I_{\text{VE-DSR}} / I_{\text{GFP}}$  ratio varied between  $1.10^5$  – to infinite (20 measurements from 5 images). From ratio-metric quantification, it can be deduced that the localization of VE-DSR or GFP-MyoX is not disturbed by GFP- and DSR- associated fluorescence, respectively.

antibodies as specified followed by horseradish peroxidase-conjugated goat anti-mouse or goat anti-rabbit immunoglobulin reagents (Sigma). The immunoreactive bands were revealed using ECL Western blot detection kit (Amersham).

#### Immunofluorescence labelling of fixed HUVECs

For all immunostainings except MyoX, cells were fixed for 20 min with 3% paraformaldehyde, permeabilized using 0.5% Triton X-100 for 3 min. Protocol to visualize MyoX is adapted from (23). Briefly, after two rinsing steps in calcium- and magnesium-containing PBS, cells kept 3 min on ice were pre-permeabilized 3 min in MyoX-Buffer (10 mM PIPES, pH 6.8, 50 mM NaCl, 3mM  $\text{MgCl}_2$ , 300 mM Sucrose) with 0.5% Triton X-100 containing an inhibitor cocktail (Roche) prior to be fixed 20 min at room temperature with chilled MyoX-Buffer containing 4% PFA. After a blocking step in 5% fetal calf serum-containing PBS during 1 hour, cells were incubated with primary antibodies overnight at 4°C and subsequently incubated with appropriate secondary antibodies.

#### Microscopy

For videomicroscopy experiments, once seeded on Lab-Tek I chambers, HUVECs and HeLa cells were maintained in phenol red-deprived-M199 (supplemented with low serum growth supplement, 20% fetal calf serum and

antibiotics) and in phenol red-deprived-DMEM (supplemented with 10% fetal calf serum and antibiotics) cell culture media, respectively. Confocal videomicroscopy images were collected on a Zeiss LSM510 confocal microscope equipped with a heating workplate, a humidifier, a  $\text{CO}_2$  delivery system and using either a  $\times 63$  Plan Apochromat objective (oil, 1.45 NA, pH 3) or a  $\times 40$  Plan-Neofluar objective (oil, 1.30 NA, pH3) (Photonic microscopy/Cellular Imaging platform of Institut Albert Bonniot, Grenoble, France). Time between images was typically 1-3 min. Phase contrast images were always co-acquired with YFP in order to reduce the delay between frames. Epifluorescence videomicroscopy images were collected sequentially on an IX71 (Olympus) microscope equipped with a heating workplate, a humidifier and a  $\text{CO}_2$  delivery system and using a  $\times 40$  Plan Apochromat (oil, 1.0 NA, pH3) or a  $\times 40$ UApochromat (oil, 1.35 NA) objectives and an ORCA-ER camera (Hamamatsu). Typical time between frames for epifluorescence videomicroscopy varies from 100 ms to 1 min. In general, cells were imaged over periods of 1-180 min. Confocal images on fixed cells were collected sequentially using a Leica TCS-SP2 confocal microscope (Leica Mannheim, Germany) equipped with a  $\times 63$  HCX Plan Apochromat objective (oil, 1.4 NA).

Epi-fluorescence images on fixed cells were acquired using an Axioplan 2 microscope (Zeiss) equipped with a  $\times 100$  Achromatic (oil, 1.25 NA) or  $\times 50$  Achromatic (oil, 0.9 NA) and an AxioCam MR camera. Fluorescence filters were chosen and tested on each combination of plasmid constructions to abolish fluorescence overlap. Only microscope proprietary softwares were used to acquire images.

### Image processing

Each time lapse confocal image corresponds to the projection of four 500 nm optical sections. Movies were treated and edited using ImageJ and Adobe After Effects 6.5 and exported using Quick Time Pro 7.4 with H.264 codec. For fixed cells, images were treated and mounted using Adobe Photoshop CS 2 and Illustrator CS 2.

### Patch velocity measurements and statistics

Kymographs were generated using ImageJ and Multiple kymograph plugin. In fact, kymographs were generated by analyzing several filopodia from different HeLa cells. Two typical kymographs illustrating the forward (A) and backward (B) movements of GFP-MyoX are shown in **Fig 4**. The two-sample *t*-test was used to determine if the average rates for forward

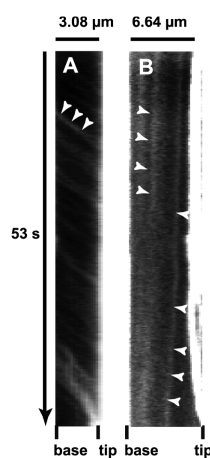


**FIG. 4.** Kymographs illustrating the forward and backward movements of GFP-MyoX. (A) Kymograph of a selected filopodium emanating from GFP-MyoX-expressing HeLa cells imaged at 25°C using a  $\times 40$  lens (N.A. 1.35), a pixel size of 162 nm, a frame rate of 5.6 images.s<sup>-1</sup> over 300 frames. Numerous faint tracks sloped down towards the filopodium tip illustrating the forward movement of GFP-MyoX. Note that patches of GFP-MyoX move at a relatively similar constant velocity. (B) Kymograph of a selected filopodium emanating from a GFP-MyoX-expressing HeLa cell imaged as in Fig 4 A. Two faint tracks sloped down towards the filopodium base illustrating the backward movement of MyoX.

movements of VE-DSR and GFP-MyoX, derived from velocity histograms were equivalent.

### Cryo-electron microscopy

HUVECs were plated on holey carbon fibronectin pre-coated nickel grids. After a 24 hour post-seeding time, cells were fixed with paraformaldehyde at room temperature. VE-Cad was then stained with the monoclonal antibody BV9 and protein A conjugated to 10 nm-colloidal gold. Cells were submitted to a post-fixation step using glutaraldehyde. For cryoEM observation of VE-Cad, grids were rapidly plunged into a liquid ethane bath cooled with liquid nitrogen (Leica EM CPC, Vienna, Austria) and maintained at a temperature of approximately -170 °C using a cryo-holder (Gatan, Pleasanton, CA) prior to be observed using a FEI Tecnai F20 electron microscope (Eindhoven, NL) operating at 200 kV under low-dose conditions. Images were recorded with a 2Kx2K low scan CCD camera (Gatan).

## RESULTS

### Filopodia establish the preliminary endothelial cell-cell contacts

To elucidate the role of filopodia in the formation of early endothelial cell-cell contacts, HUVEC monolayers were co-stained for VE-cadherin and actin. As expected, it revealed that the most mature junctions exhibited a continuous thin VE-Cad labelling close to circumferential actin cables (**Fig 5**, middle and upper panels). But, in preliminary cell-cell contacts, VE-Cad labelling exhibited a characteristic zigzag staining dotted with residual randomly distributed intercellular gaps (**Fig 5**, middle and lower panels). These newly formed intercellular contacts were composed of multiple protrusions where VE-Cad co-localized with radially oriented actin fibers (**Fig 5**, lower panels). Cryo-electron microscopy confirmed and showed more precisely that, in subconfluent HUVECs, VE-Cad molecules are distributed along and at the tips of protrusions. The electron micrographs also revealed the presence of actin filaments aligned in tight parallel bundles within these protrusions that, consequently, could be functionally defined as filopodia (**Fig 6**)(34).

### VE-Cad molecules navigate on filopodia

We then used videomicroscopy to examine whether VE-Cad is able to move along filopodia. To visualize VE-Cad, various constructs coding for VE-Cad C-terminally fused to fluorescent DsRed (red), YFP (yellow), CFP (cyan) proteins were elaborated to express VE-DSR, VE-YFP or VE-CFP, respectively (**Fig 2**). It must be noted that these cDNA constructs were designed to produce fluorescent VE-Cad molecules that remained monomeric and interact with catenins (report to Materials and Methods, **Fig 2**).

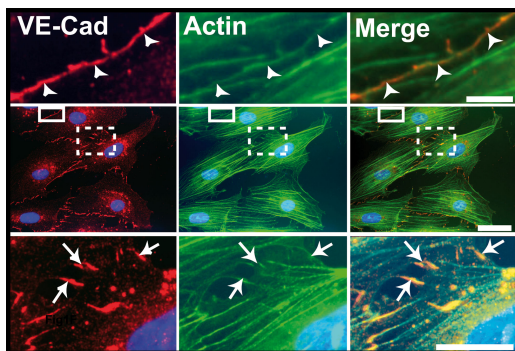


**FIG. 5.** Localization of VE-Cad in subconfluent HUVECs. Images on the central row show a HUVEC monolayer immunolabelled for VE-Cad (red, left), actin (green, centre) and merge (right). The selected enlargements of a mature cell-cell junction (continuous frame) and an immature junction (dotted frame) are shown at the upper and lower rows, respectively. In mature junctions, VE-Cad and cortical actin fibers are located at the cell circumference (arrow-heads, upper row). By contrast, in immature junctions, VE-Cad co-localizes with radial actin fibers along filopodial extensions bridging adjacent cells (arrows, lower row). Bars: 2  $\mu\text{m}$  (upper); 10  $\mu\text{m}$  (middle) and 5  $\mu\text{m}$  (lower).

At subconfluency, HUVECs emitted numerous filopodia that formed bridges between neighbouring cells (**Fig 5**). In preliminary confocal videomicroscopy experiments performed on VE-YFP-expressing HUVECs, at a frame rate of 1 image.min<sup>-1</sup>, we observed that some patches of VE-YFP adopted linear trajectories by moving along pre-established filopodia (**Fig 7**, **See supplementary data, Movie 1**). By contrast, no such movement was seen for YFP (**Fig 7**, **See supplementary data, Movie 2**). In a second type of experiments, sparse living HUVECs transiently expressing VE-DSR were observed by videomicroscopy using a frame rate of 3 images.s<sup>-1</sup> (**Movie 3**). Under these conditions, isolated cells emitted numerous free filopodia along which faint VE-DSR particles moved rapidly. VE-DSR trajectories appeared nearly linear and were more

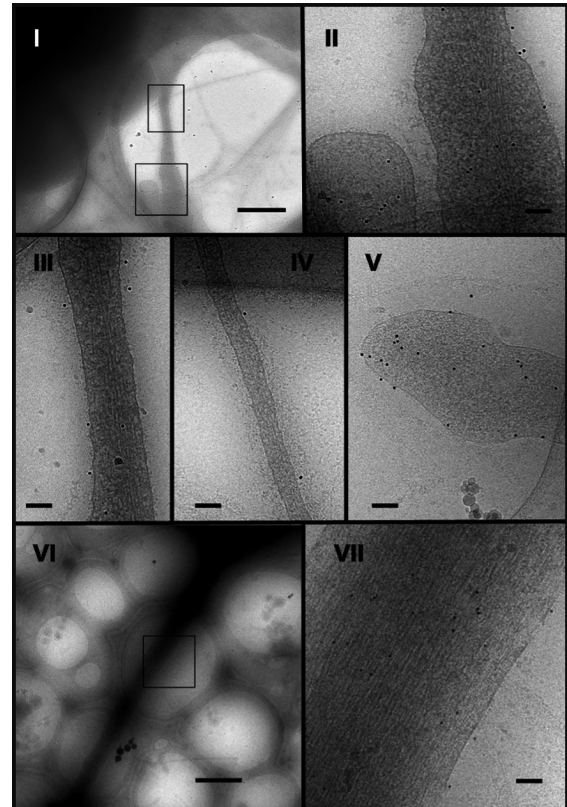


**FIG. 6.** Localization of VE-Cad at the surface of HUVEC filopodia by electron microscopy. Living HUVECs were seeded on electron microscopy holey grids and grown for 24 hours. After fixation without permeabilization, cells were successively marked with mAb BV9 antibody and protein-A gold particles to reveal the presence of VE-Cad at the cell surface. They were then vitrified for observation. Electron micrographs revealed filopodia of various diameters and lengths connecting adjacent cells (micrographs I and VI, bars = 1  $\mu\text{m}$ ). Higher-magnification images show gold particles dispersed along the length (micrographs II, III, IV and VII; bars = 100 nm) and at the tip of filopodia (micrograph V; bar = 100 nm). This indicates that VE-Cad is distributed over the surface of filopodia. Furthermore, on large as well as thin filopodia, underneath the plasma membrane, the network of actin fibers could be observed parallel to the filopodium axis (micrograph VII).

rapid in **Movie 3** than those observed by slow frame rate confocal videomicroscopy in **Movie 1**. By contrast, such a rapid traffic was not observed in HUVECs overexpressing control DsRed (**Movie 4**), thereby indicating that trafficking is due to the VE-Cad moiety linked to the transportation machinery. Altogether, the data suggest that VE-Cad molecules navigate on filopodia probably

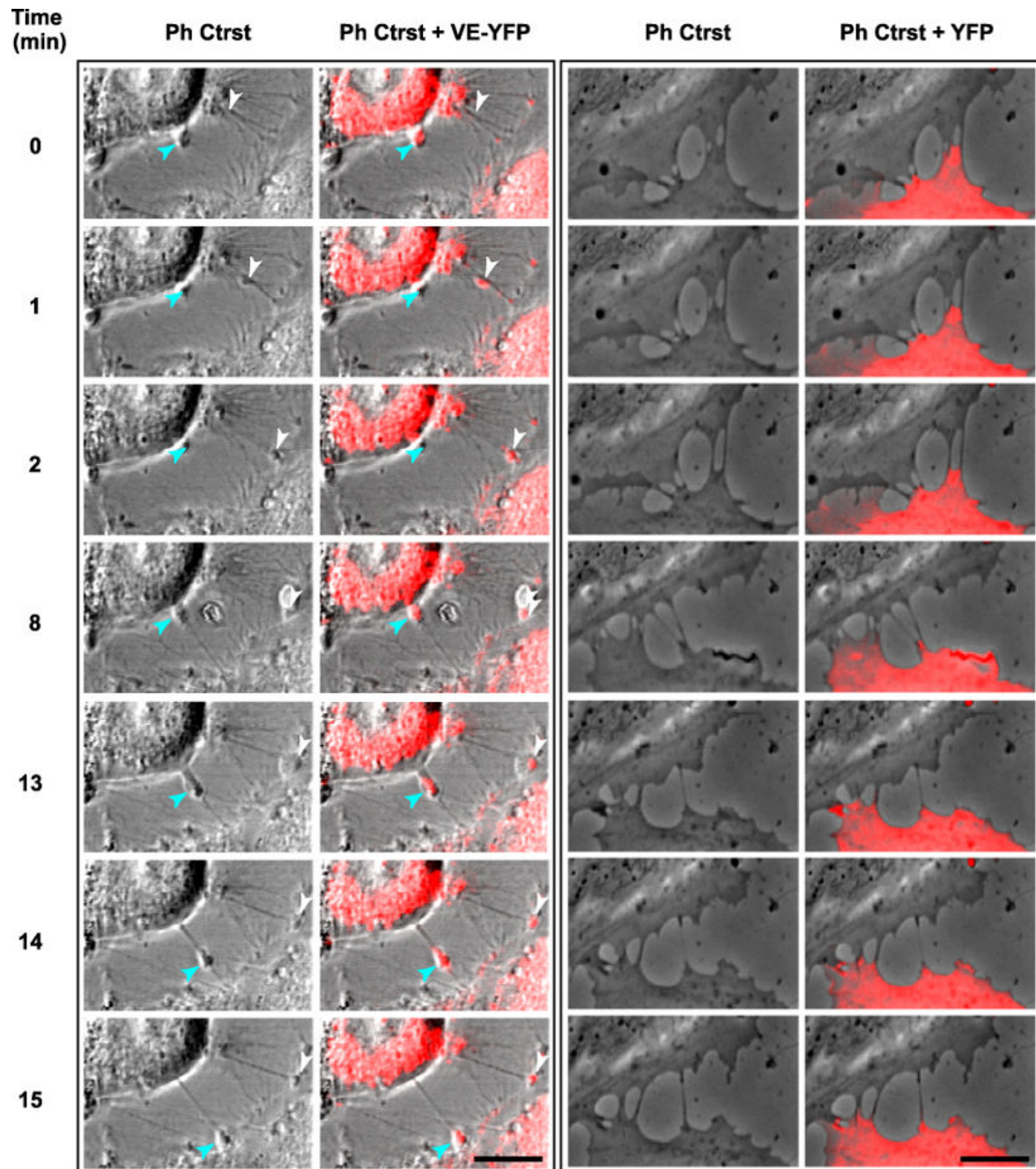


FIG. 7. Selected sequences showing VE-YFP moving along filopodia. Subconfluent HUVECs were transiently transfected with the plasmids expressing either VE-YFP or YFP. At 17 h post transfection time, confocal videomicroscopy images were taken every min for 1 hour both in phase contrast to see the filopodia and in the yellow fluorescence channel. Panels corresponding to VE-YFP-expressing HUVECs (Left) showed two distinct patches, indicated by arrow-heads, moving sequentially along two filopodia. Report to Movie 1 in Supplementary data. By contrast, no YFP was detected along filopodia as illustrated in panels corresponding to YFP-expressing HUVECs (right). Report to Movie 2 in Supplementary data. Bars = 10  $\mu$ m

through an actin-dependent mechanism excluding the possibility that membrane diffusion be at the basis of VE-Cad motion. Moreover, as shown thereafter, the fast and slow velocities observed for VE-Cad particles corresponded to forward (towards the filopodium tip) and backward (towards the filopodium basis) motions respectively.

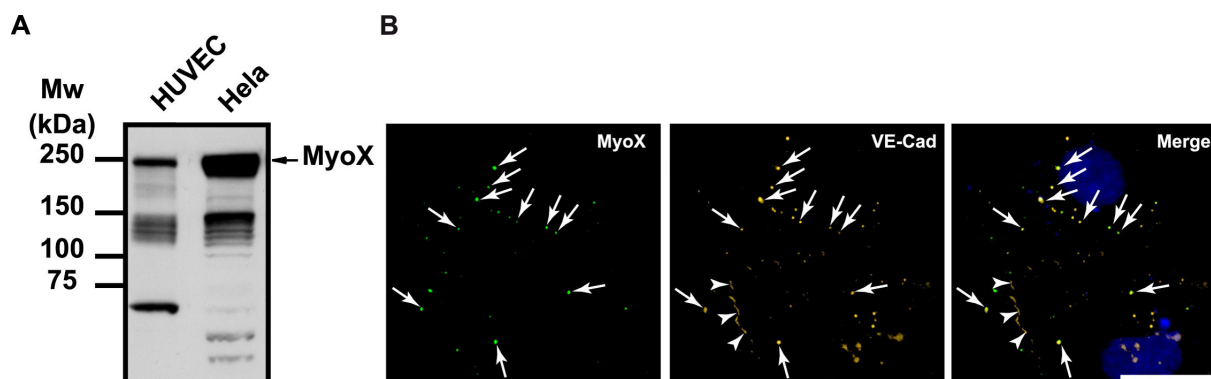


FIG. 8. Expression of MyoX in HUVEC and HeLa cells. (A) Detection of endogenous MyoX by Western blot. HUVEC and HeLa lysates were analysed by Western blot using the anti-MyoX pAb antibody. In HUVECs as well in HeLa, the antibody detected a 240 kDa band corresponding to the expected size of MyoX and several bands of lower molecular mass corresponding to MyoX degradation (6). Higher amounts of MyoX were detected in HeLa cells compared to HUVECs. (B) Partial co-localization of endogenous MyoX and VE-Cad along filopodia in subconfluent HUVECs. Subconfluent HUVECs were double labelled for MyoX (left) and VE-Cad (centre) with pAb anti-MyoX, mAb anti-VE-Cad BV9, Alexa-555-labelled goat-anti-rabbit and Alexa-488-labelled goat-anti-mouse antibodies and Hoescht. The merged image is at the right. Arrows pointed out VE-Cad patches co-localized with MyoX while arrowheads indicated cell-cell junctions where VE-Cad and MyoX did not co-localize. Bar: 20  $\mu$ m.

### The motor protein myosin-X interacts with the VE-Cad-catenin complex

As VE-Cad is able to move along filopodia, we hypothesized that VE-Cad is directly or indirectly linked to intrafilopodial actin fibers through an actin motor protein. Myosins constitute a family of actin-dependent motor proteins that support protein carrier function. Endothelial cells expressed several myosin family members such as myosin-II, -VII and -X. The unconventional myosin-X (MyoX) is a potential candidate for VE-Cad transport since it is located at the filopodium tips of various non-endothelial cell lines (5).

Analysis of HUVEC lysates by Western blot using anti-MyoX antibody revealed the presence of a 240 kDa band corresponding to full-length MyoX (Fig 1 and 8 A). Additional bands with molar weights ranging 100-130 kDa were also detected because of MyoX susceptibility to proteolysis (6). Immunofluorescence labeling of subconfluent HUVECs effectively showed a punctuate staining of MyoX that partially co-localized with VE-Cad (Fig 8 B). After a careful scrutiny of immunofluorescence images, MyoX appeared associated with extrajunctional VE-Cad and not with junctional one (Fig 8 B).

We speculated that MyoX interacts, at least temporarily, with VE-Cad thus allowing its

cellular transport along intrafilopodial actin fibers. To verify this hypothesis, different approaches such as immunoprecipitation and pull-down assays were used. Hence, analyses of VE-Cad immunoprecipitates by Western blot using an anti-MyoX antibody revealed the presence of the 240 kDa form of MyoX (Fig 9 A). Conversely, anti-MyoX immunoprecipitation showed association of MyoX with the uncleaved form of VE-Cad (Fig 9 B). To confirm immunoprecipitation data, GST pulldown assays were performed on HUVEC extracts using the FERM (band 4.1 Ezrin, Radixin, Moesin) domain of MyoX previously described to be involved in cargo binding (43), (28) and N-terminally-coupled to GST (GST-FERM). The GST-FERM fusion protein was first assayed for its capacity to bind integrin  $\beta$  chains, as

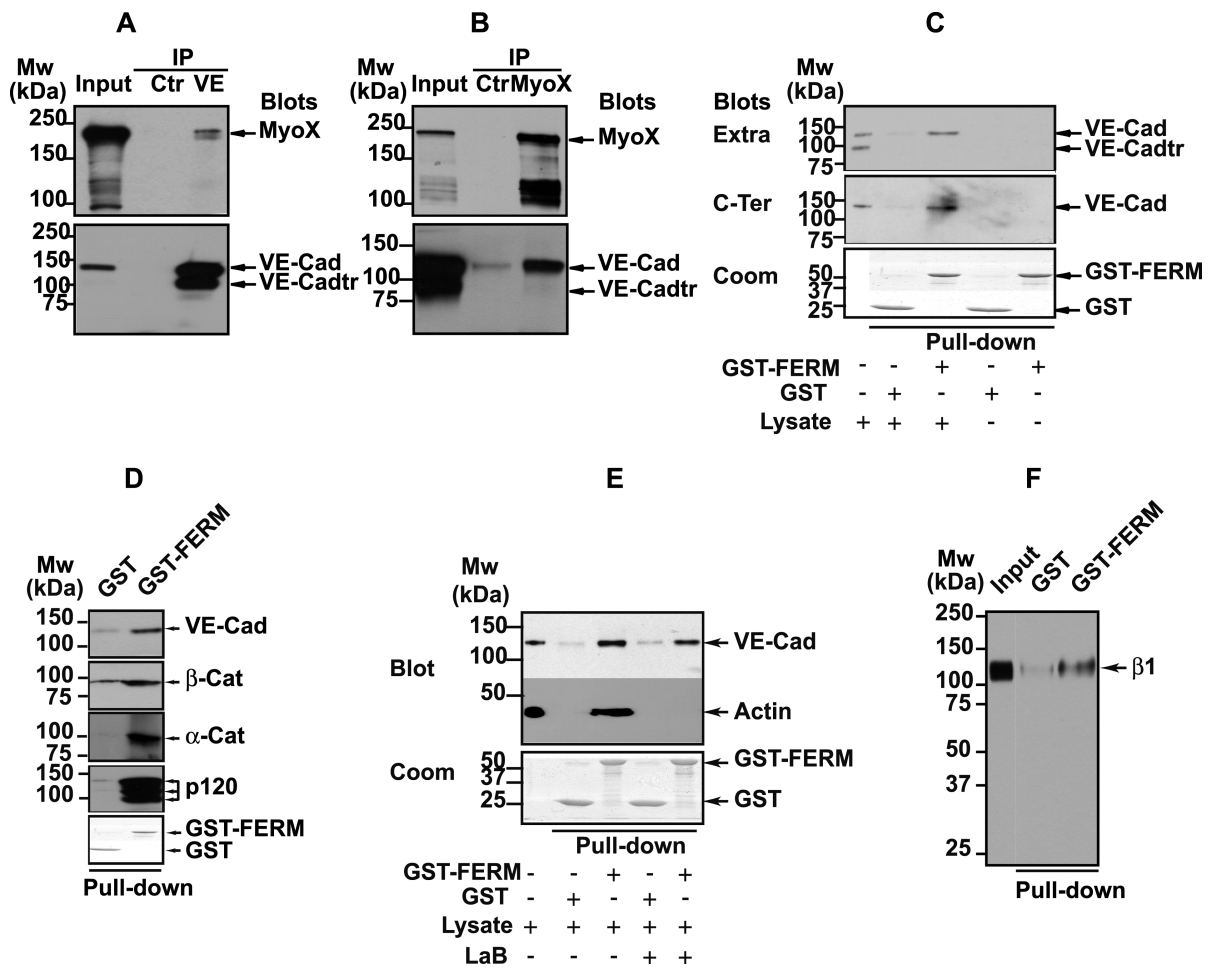


FIG. 9. Association of MyoX to the VE-Cad-based complex. (A, B) Co-immunoprecipitations of endogenous MyoX with endogenous VE-Cad in HUVECs. Anti-VE-Cad (IP VE, A) and anti-MyoX (IP MyoX, B) immunoprecipitations were resolved on 4-12% gradient gels, electro-transferred and probed successively for VE-Cad and MyoX. As controls, an aliquot of whole cell lysate (input) and immunoprecipitations performed on HUVEC lysates using rabbit non-immune IgG (Ctr) were analyzed in parallel. Note that Anti-VE-Cad IP (A) and input analysis by Western blot (B) revealed the presence of a 100 kDa truncated form of VE-Cad (VE-Cadtr). Molecular weight markers are given at the margins of each panel. (C) Interaction of MyoX with the VE-Cad complex through its FERM domain. GST or GST-FERM immobilized on glutathione beads was incubated with either HUVEC lysates or with buffer. Pull-down assays were revealed with the anti-VE-Cad antibodies directed against the extracellular domain (Extra, mAb BV9) or the cytoplasmic domain (C-Ter, pAb C-19). Lower panel: Coomassie staining of GST proteins used in each pull-down assay. For comparison, aliquots of whole cell lysates and pull-down assay controls performed without lysate were analyzed in parallel. Note that the antibody C-19 raised against the 19 amino acid C-terminal peptide of VE-Cad did not recognize VE-Cadtr indicating that the truncated form of VE-Cad is cleaved at its C-terminus. Only the uncleaved form of VE-Cad is co-precipitated with the FERM domain of MyoX. (D) Co-precipitation of catenins with VE-Cad by the FERM domain of MyoX. GST and GST-FERM pull-down assays performed on HUVEC lysates were probed with VE-Cad,  $\alpha$ -catenin ( $\alpha$ -cat),  $\beta$ -catenin ( $\beta$ -cat) and p120 antibodies. All these proteins were detected in pull-down assays performed with GST-FERM but not with GST alone. (E) The interaction between the VE-Cad complex and MyoX does not require actin fibers. GST and GST-FERM pull-down assays performed on HUVEC lysates treated (+) or not (-) with latrunculin B (LaB) were sequentially immunoblotted for VE-Cad with C-19 pAb and for  $\beta$ -actin with anti- $\beta$ -actin mAb. For comparison, an aliquot of whole cell lysate was analyzed in parallel. Lower panel: Coomassie staining of GST proteins. In pull-down assays, VE-Cad was precipitated with the domain FERM of MyoX even in the absence of actin. (F) The recombinant GST-FERM protein interacts with the  $\beta$ 1 chain of integrins. GST and GST-FERM pull-down assays performed on HUVEC lysates were immunoblotted for the  $\beta$ 1 chain of integrins with the pAb anti- $\beta$ 1 integrin antibody. For comparison, an aliquot of whole cell lysate (Input) was analyzed in parallel. In pull-down assays,  $\beta$ 1 chain of integrins was precipitated with the domain FERM of MyoX.

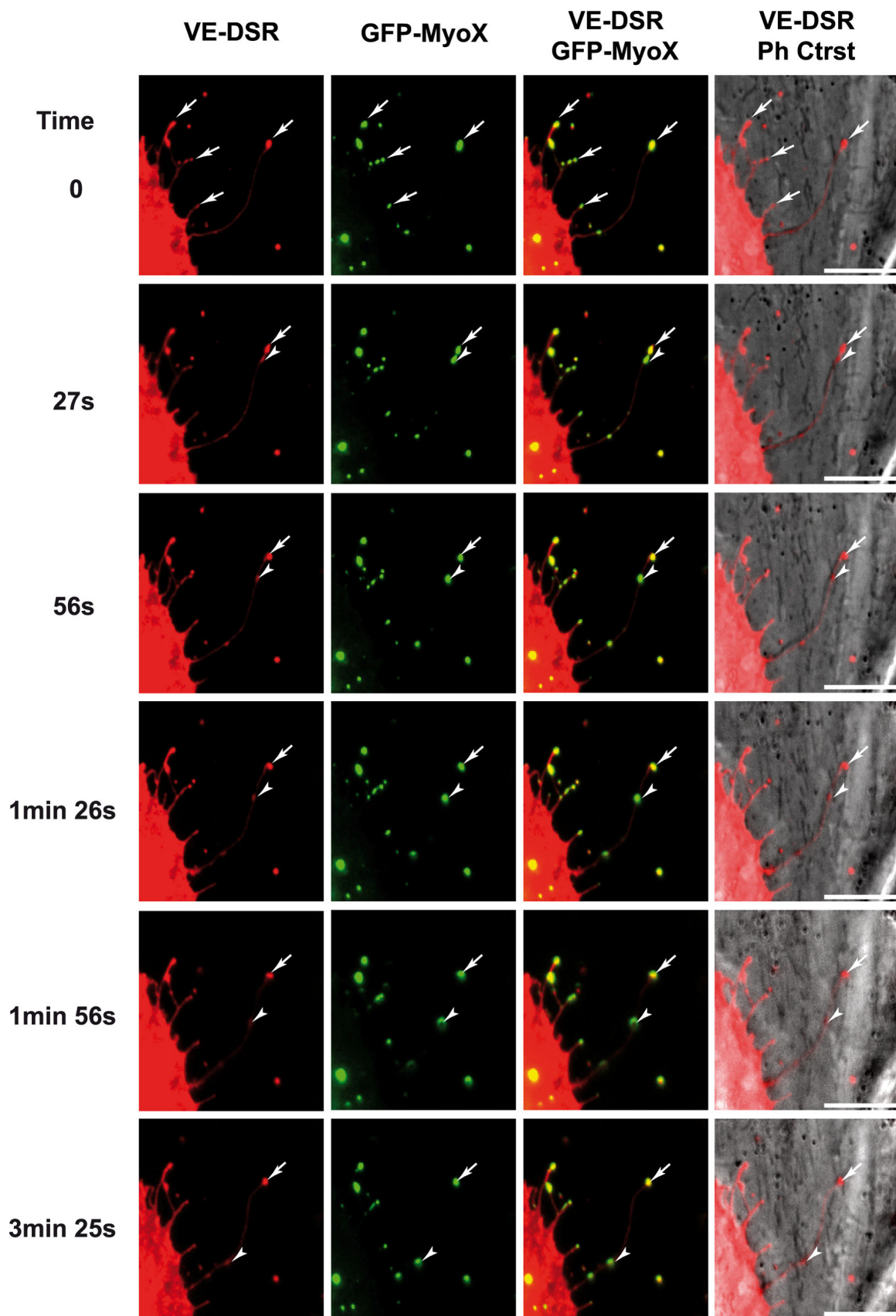


FIG. 10. Selected sequence focusing on the coordinated backward movements of MyoX and VE-Cad. Subconfluent HUVECs, transiently co-transfected with plasmids expressing GFP-MyoX and VE-DSR, were observed by videomicroscopy at 17 h post transfection at a frame rate of 1 image/ 3s. Full arrow-heads and arrows indicate moving and immobile patches, respectively, for VE-Cad and MyoX. Bars = 10  $\mu$ m.

previously reported for MyoX (41). Pull-down assays, performed on HUVEC extracts, revealed that GST-FERM retained the capability to interact with the integrin  $\beta$ 1 chain whereas GST did not (Fig 9 F). Importantly, GST-FERM specifically interacted with the uncleaved 135 kDa form of VE-Cad and not with the intracellular truncated 100 kDa form present in HUVEC lysates (Fig 9 C). Moreover, GST-FERM was able to pull down the VE-Cad cytoplasmic partners  $\alpha$ -,  $\beta$ - or p120- catenins from HUVEC lysates (Fig 9 D). By contrast, it did not interact with a recombinant fragment that overlapped the amino stretch A630-Y784 corresponding to the cytoplasmic region of VE-Cad truncated at its N-terminus (40) (data not shown). This indicates that MyoX associates with one element of the VE-Cad-catenin complex without disturbing its integrity. In addition, actin, probably incorporated in filaments, was also co-precipitated with GST-FERM and not with GST (Fig 9 E). To exclude the possibility that actin filaments link the VE-Cad-catenin complex to MyoX, filaments were depolymerized in cell extracts with the actin monomer-sequestering drug latrunculin B (LaB) (13). In these conditions, no actin was precipitated in GST-FERM pull-down assays (Fig 9 E). However, VE-Cad was still pulled-down with GST-FERM indicating that actin cables were not involved in the link between the VE-Cad-catenin complex and MyoX. Finally, substitution in pull-down assays of the FERM domain of MyoX by the FERM domain of moesin did not precipitate VE-Cad attesting that the results obtained with the FERM domain of MyoX are specific (Data not shown). Altogether, our results establish that the FERM domain of MyoX interacts with the VE-Cad-catenin complex.

### **MyoX transports VE-Cad along filopodia**

To examine the temporal and spatial co-localization of VE-Cad and MyoX, VE-DSR

and MyoX N-terminally fused with GFP (GFP-MyoX (6)) were co-expressed in HUVECs. We first controlled the specificity of the localization of VE-DSR and GFP-MyoX prior to imaging (Fig 3). Using videomicroscopy, we noticed that some patches of GFP-MyoX remained immobile at filopodium tips while others started from the tips of filopodia dragging VE-DSR clusters backwards (Fig 10, See Supplementary data, Movie 5). This backward movement was relatively slow and could be observed by videomicroscopy using a frame rate of 1 image/ 3 s. In addition, movements of VE-DSR and MyoX patches towards the tips of filopodia (forward motion) were also observed. But, the high displacement rate at 37°C in HUVEC rendered the observation of these movements difficult. To palliate this inconvenience, we chose to image VE-DSR and GFP-MyoX motilities in HeLa cells. These experiments were performed at 25°C to reduce the movement rate (21) since HeLa cells, by contrast to HUVECs, tolerate this temperature. Under these selected conditions, HeLa exhibited 10-20  $\mu$ m long filopodia and it was possible to individually track VE-DSR and GFP-MyoX patches over times ranging 50-100 s (See Supplementary data, Movies 6 and 7). Hence, Movie 7 shows a single patch of GFP-MyoX that co-localized with a single VE-DSR patch and moved synchronously with it on a given filopodium. Both patches moved backwards prior to moving towards the distal tip of the filopodium (full arrow-heads). It could be noticed that the backward movement was frequently interrupted by episodes of pausing (See Supplementary data, Movie 7). Movie 7 also highlights the difference existing between forward and backward velocities. Altogether, our results on MyoX and VE-Cad co-localization and co-migration along

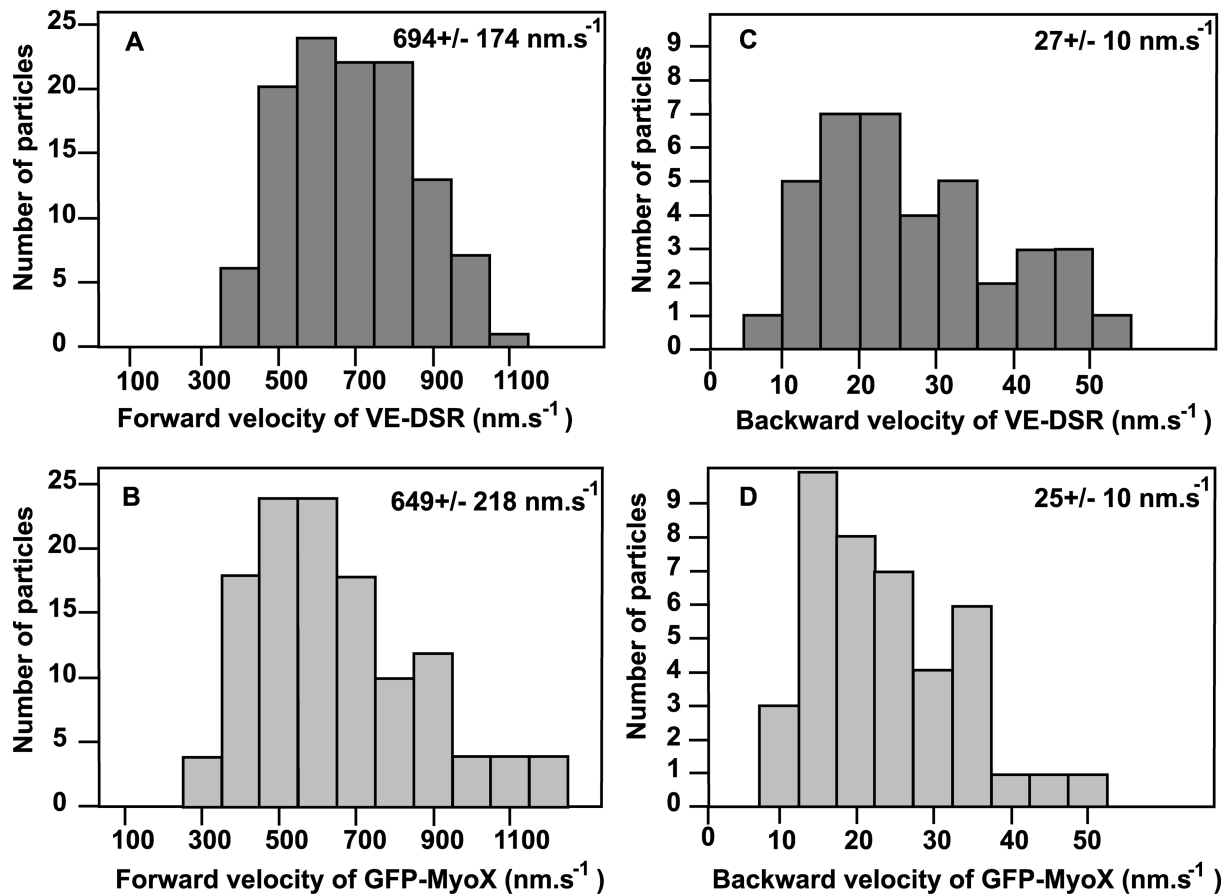


FIG. 11. Velocity histograms for forward and backward movements of VE-DSR and GFP-MyoX patches. Histograms corresponding to the forward movements of VE-DSR (A) and GFP-MyoX (B) patches were generated from 115 and 129 measurements respectively while those corresponding to the backward movements of VE-DSR (C) and GFP-MyoX (D) patches from 38 and 41 measurements respectively. At the top right, the means  $\pm$  standard deviations are indicated. HeLa cells were imaged at 25°C using a  $\times 40$  lens (N.A. 1.35), a pixel size of 162 nm and a frame rate ranging 3-5 images.s<sup>-1</sup>.

filopodia strongly suggest that VE-Cad is transported by a MyoX-dependent mechanism.

Frequently, VE-DSR / GFP-MyoX patches moving forward and backward were individually observed on the same filopodium. To obtain a global vision of protein movements along a given filopodium, location of each individual patch was plotted versus time to generate a kymograph. In this kind of projection, each patch movement appears as an individual line directed towards the tip of filopodium for forward movement and towards filopodium base for backward movement (Fig 4). The velocity of a large number of individual patches visualized by single-channel videomicroscopy could be derived from the slope of the tracks in kymographs and reported in histograms showing the velocity profile for

each fusion protein (Fig 11). Hence, we calculated that VE-DSR moved at an average forward rate of 694  $\pm$  174 nm.s<sup>-1</sup> (115 measurements on 35 filopodia)(Fig 11 A) and at an average backward rate of 27  $\pm$  10 nm.s<sup>-1</sup> (38 measurements on 22 filopodia) (Fig 11 C). Similarly, GFP-MyoX kymographs showed that GFP-MyoX moved forward at an average velocity of 649  $\pm$  218 nm.s<sup>-1</sup> (129 measurements on 15 filopodia) (Fig 11 B) and backwards at 25  $\pm$  10 nm.s<sup>-1</sup> (41 measurements on 22 filopodia) (Fig 11 D) as previously described (21). Statistically, according to the two-sample *t*-test, the mean rates for the forward movements of VE-DSR and GFP-MyoX are equivalent ( $p > 0.05$ ).

Double-channel videomicroscopy experiments were also performed on HeLa co-expressing GFP-MyoX and VE-DSR to visualize the synchronous movements of the two fluorescent proteins. Hence, in **Fig 12 A and B**, dual kymographs showed two selected GFP-MyoX and VE-DSR particles that exhibited synchronous backward (pointed out by arrowheads) and forward (pointed out by arrows) motions. These experiments confirm the co-transport of GFP-MyoX and VE-DSR along filopodia in both directions. Because of the known functions of MyoX as a cargo for protein transport and as an actin motor protein, it is likely that MyoX mediates the transportation of the VE-Cad complex along intrafilopodial actin cables.

#### MyoX FERM domain overexpression blocks the transportation of VE-CFP

We next tried to test the functional role of MyoX-mediated transport of VE-Cad. We opted for a dominant-negative approach by constructing the fusion GST-FERM-DSR protein consisting of the GST moiety, the FERM domain of MyoX and DSR (**Fig 13 A**). This fluorescent protein was designed to retain the cargo function but to remove the motor function of MyoX. The fusion protein GST-DSR, composed of the GST and the DSR entities, was also elaborated and used as a control (**Fig 13 A**). The cDNA constructs coding for GST-FERM-DSR and GST-FERM were transiently transfected in CHO cells and the expression of recombinant proteins was analyzed by Western blot using the polyclonal anti-GST antibody. As expected, a 110 kDa and a 80 kDa bands were detected in the GST-FERM-DSR and GST-DSR transfectants, respectively (**Fig 13 B**). Moreover, GST-FERM-DSR interacted with VE-Cad as attested by immunoprecipitation experiments performed on CHO cells co-expressing VE-Cad and GST-FERM-DSR. By contrast, GST-DSR did not (**Fig 13 C**).

To prove that VE-Cad sequestration by GST-FERM-DSR is specific, we co-

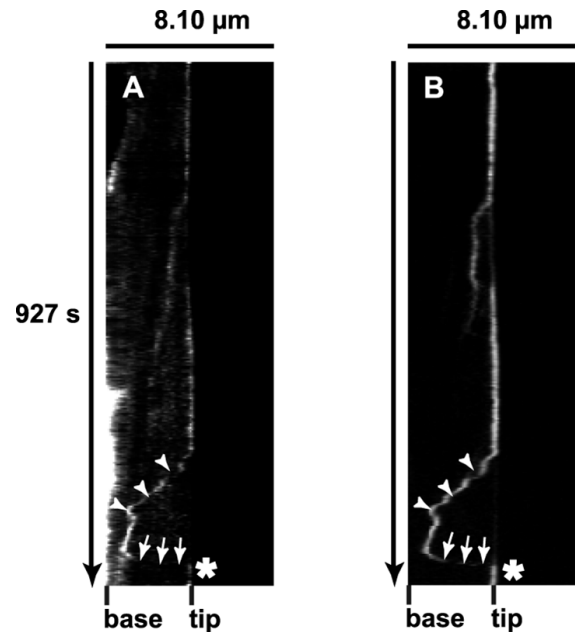


FIG. 12. MyoX and VE-Cad dynamics in living HeLa cells. Synchronous kymographs of a selected filopodium emanating from HeLa cells co-expressing VE-DSR (A) and GFP-MyoX (B) imaged at 25°C using a 40x lens (N.A. 1.35), a pixel size of 162 nm and a frame rate of 3 images / 10s. The VE-DSR kymograph showed a patch that (1) remained stationary (vertical track), (2) globally moved backward towards the filopodium base (arrowheads), (3) abruptly changed of direction, and (4) moved forward (arrows) prior to reach the filopodium tip. Note that the backward phase was frequently interrupted by pausing events, thus creating a stair-shaped track (arrowheads). This track was perfectly detected in the corresponding GFP-MyoX kymograph illustrating the synchronous movement of VE-DSR and GFP-MyoX patches on a given filopodium.

transfected VE-Cad-expressing CHO cells with plasmids coding for GFP-MyoX and either GST-DSR or GST-FERM-DSR. Anti-MyoX immunoprecipitations on cell lysates revealed that the amount of VE-cadherin co-precipitated with MyoX remained nearly unchanged in the presence or absence of GST-DSR (**Fig 13 D**). By contrast, a slight and reproducible decrease in the VE-Cad amount immunoprecipitated with MyoX was observed in the presence of GST-FERM-DSR suggesting that GST-

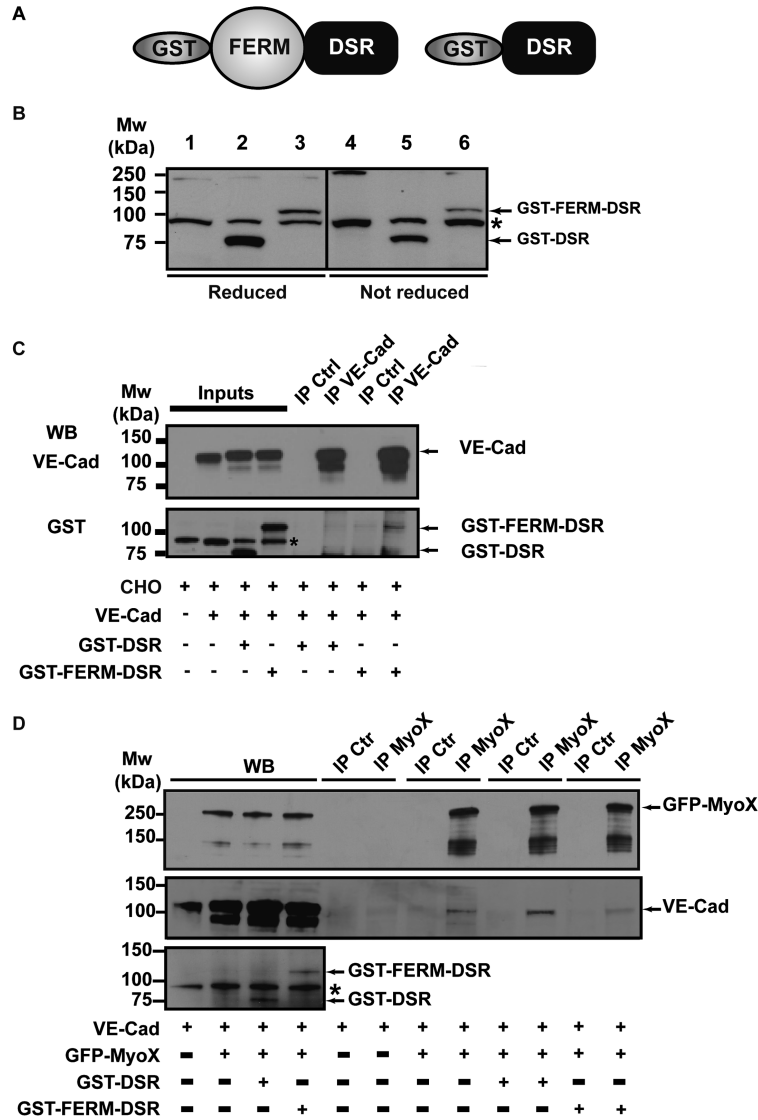


FIG. 13. Biochemical characterization of the recombinant proteins GST-FERM-DSR and GST-DSR. (A) Schematic representation of MyoX and its derived fragments. The recombinant fragment GST-FERM-DSR was designated to keep the capacity of MyoX to interact with VE-Cad via its FERM domain. The GST-DSR recombinant fragment was used as a control. (B) Expression of GST-DSR and GST-FERM-DSR. CHO cells were transfected with either GST-DSR (lanes 2 and 5) or GST-FERM-DSR (lanes 3 and 6) or not (lanes 1 and 4). Expression of GST-DSR and GST-FERM-DSR in CHO cells was verified by Western blot using the anti-GST antibody. This antibody recognized a 80 kDa and a 110 kDa bands corresponding to GST-DSR and GST-FERM-DSR, respectively. Additionally, it also unspecifically recognized a protein present in CHO lysates (star). (C) GST-FERM-DSR interacts with VE-cadherin. Anti-VE-Cad immunoprecipitations (IP VE-Cad) were performed on CHO cell lysates co-expressing either VE-Cad and GST-FERM-DSR or VE-Cad and GST-DSR using the mAb anti-VE-Cad BV9. As controls, aliquots of whole CHO lysates (inputs) and immunoprecipitations performed on CHO lysates using mouse non-immune IgG (IP Ctrl) were analyzed in parallel. A 110 kDa band corresponding to GST-FERM-DSR was detected in the anti-VE-Cad immunoprecipitate, indicating that GST-FERM-DSR is able to interact with VE-Cad. The anti-GST antibody recognized as in **Fig 13 B** GST-DSR and GST-FERM-DSR as well as an unspecific protein present in CHO cell lysates (star). Molecular weight markers are given at the left margin. (D) Cellular VE-Cad sequestration by MyoX FERM domain. VE-Cad-expressing CHO cells (40) were transiently transfected with plasmids coding for GFP-MyoX and either GST-DSR or GST-FERM-DSR. After cell lysis, Anti-MyoX immunoprecipitations were resolved on 4-12% gradient gels, electrotransferred and probed successively for VE-Cad, MyoX and GST. As controls, aliquots of the various CHO lysates and immunoprecipitations performed using rabbit non-immune IgG (IP Ctrl) were analyzed in parallel. Molecular markers are given at the margin of each panel.

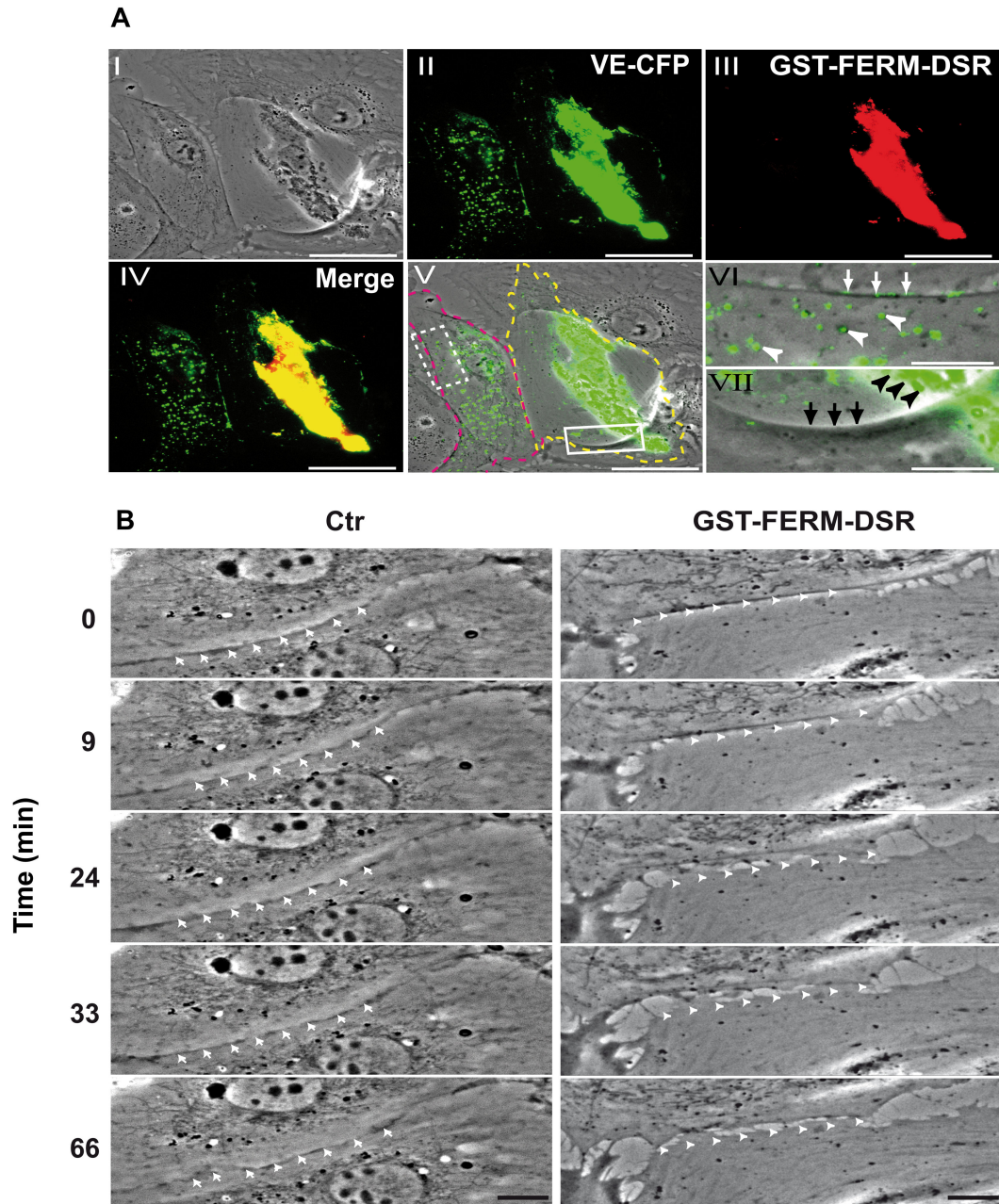


FIG. 14. Functional role of MyoX-mediated transport of VE-Cad. (A) Blockage of VE-CFP transport by GST-FERM-DSR expression. Subconfluent HUVECs transiently co-transfected with plasmids expressing VE-CFP and GST-FERM-DSR were observed 20 h post transfection in phase contrast (I) and in the cyan and red fluorescence channels. VE-CFP (II, green), GST-FERM-DSR (III, red), VE-CFP and GST-FERM-DSR merging (IV) and VE-CFP and phase contrast merging (V, VI and VII) allowed the visualisation of two adjacent differentially-transfected cells: the cell at the right (delimited by yellow dotted line) co-expressed GST-FERM-DSR and VE-CFP while the cell at the left (delimited by pink dotted line) only expressed VE-CFP. Other cells of the fields are untransfected. The selected enlargements show that VE-CFP patches are at the cell-cell-junctions (white arrows) and dispersed at the cell surface (white arrow-heads) in monotransfected cell (VI-dotted rectangle in V) whereas in the double transfected cell, VE-CFP and GST-FERM-DSR co-localized and gathered around the cell nucleus (black arrow-heads, VII- rectangle in V) indicating that GST-FERM-DSR blocked the VE-Cad transport to the cell edge. In control experiments, in cells co-expressing GST-DSR and VE-CFP, VE-CFP patches are located at cell-cell-junctions (data not shown). Bars = 40  $\mu$ m (I to V); 10  $\mu$ m (VI and VII). (B) Blockage of intercellular contact formation by GST-FERM-DSR expression. The sequences are selected from Movie 9 and focus on the edges of two adjacent cells. In the right column, the cell below expressed GST-FERM-DSR while the cell at the top is untransfected. In the left column, both cells expressed GST-DSR. Arrow-heads show unstable junctions whereas arrows point out stable junctions. Bars = 10  $\mu$ m.

FERM-DSR competes with MyoX for interacting with VE-Cad.

Then, the cellular effect due to VE-Cad sequestration by the FERM domain of MyoX was analyzed in HUVECs co-expressing VE-CFP and GST-FERM-DSR. In double-transfected cells, VE-CFP remained static, concentrated at the periphery of the nucleus whereas, in absence of GST-FERM-DSR, VE-CFP appeared highly mobile, disseminated over the cell surface and at cell-cell junctions (**Fig 14 A, See Supplementary data, Movie 8**). We also demonstrated that GST-FERM-DSR concentrates endogenous VE-Cad in the perinuclear area while GST-DSR did not (**data not shown**). It can be deduced that, by competing with endogenous MyoX, GST-FERM-DSR could block the transportation of endogenous and exogenous VE-Cad along actin fibers. The absence of transport resulted in an almost total VE-Cad depletion at cell edges (**Fig 14 A**). Furthermore, cell-cell contacts between GST-FERM-DSR-expressing cells did not stabilize, in spite of the membrane apposition between neighbouring cells (**Fig 14 B, See Supplementary data, Movie 9**). Numerous intercellular gaps appeared and spaces between opposed cells increased with time. Hence, blockage of MyoX-mediated VE-Cad traffic prevents the adhesion between cell fronts and formation of early cell-cell contacts required for the elaboration of interendothelial junctions.

#### **MyoX/VE-Cad co-travelling operates during wound healing**

To obtain additional information about the cellular role of MyoX/ VE-Cad co-trafficking, we performed *in vitro* wound-healing assays on GFP-MyoX- and VE-Cad-DSR-overexpressing HUVEC monolayers and followed the early steps of cell-cell junction reconstruction by phase contrast and fluorescence videomicroscopy (**See Supplementary data, Movie 10**). **Movie 10** focused on two non-interacting cells, both co-expressing VE-DSR and GFP-MyoX. These cells emitted very dynamic filopodia. Clearly, several of them operated cooperatively in a confined area to constitute the first cell-cell contacts. At this specific point, it could be observed that VE-Cad accumulated at the

filopodium tips elaborating homophilic interactions as soon as filopodia touched the neighbouring cell. These very unstable preliminary cell-cell contacts initiated the formation of filopodium-based bridges between the adjacent cells. VE-cadherin-based contacts progressively distributed along the cell edges. The multiplicity of the contact points contributed to cell-cell tightening and to the reduction of the intercellular spaces leading to a stabilization of the cell-cell junction. In conclusion, these data underlined the role played by MyoX-mediated accumulation of VE-Cad at the tips of filopodia in the elaboration of preliminary endothelial cell-cell contacts, which further progress into wound closure.

#### **DISCUSSION**

In the present manuscript, we show how the actin cytoskeleton supports VE-Cad transport along filopodia to eventually elaborate primary cell-cell contacts. Indeed, we observed the to- and -fro movements of VE-Cad patches along filopodia and established that this traffic is governed by the motor protein MyoX. A model recapitulating VE-Cad movement modes is proposed in **Fig 15**.

Herein, we observed by immunofluorescent staining (**Fig 5**) and cryo-electron microscopy (**Fig 6**) that VE-Cad is located along filopodia emanating from sparse endothelial cells or forming bridges between neighbouring cells. This contrasts with the usual localization of VE-Cad at cell-cell junctions in confluent endothelial monolayers. By videomicroscopy, we uncovered that VE-Cad navigates along these filopodia (**Movies 1, 3, 5 and 6**) and suspected that a motor protein of the myosin family might be involved in this traffic. Among myosin proteins, myosin-X was a potential candidate for governing VE-Cad motions.

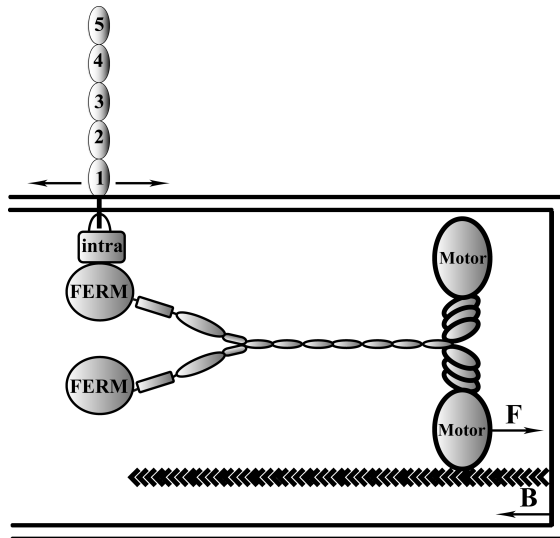


FIG. 15. Schematic model illustrating the movements of VE-Cad along filopodia (modified from (43)). MyoX binds to actin filaments via its motor domain and to the VE-Cad-catenin complex (intra) via its FERM domain. Consequently, VE-Cad moves forward (F) towards the filopodium tip at a rate ranging  $700 \text{ nm.s}^{-1}$  and backwards (B) at a rate ranging  $30 \text{ nm.s}^{-1}$ .

This unconventional motor protein is widely expressed in a variety of vertebrate tissues in particular in vascularised ones such as lung, heart and placenta (6). Consistent with this observation, MyoX was recently found in the endothelium where it is involved in cell migration guidance (28). In different cell types, it is detected along the leading edge of lamellipodia (33) but, more frequently, at the tips of filopodia. In fact, MyoX is probably involved in the initiation of filopodium formation (9, 37). It moves along filopodial actin cables by an ATP-dependent walking mechanism towards the filament barbed ends, but also towards the cell body using the actin retrograde flow (5),(6),(26). MyoX possesses a FERM domain known to interact with the  $\beta$ -chains of integrins (43). Herein, we show that MyoX associates, via its FERM domain, with the VE-Cad-catenin complex (Fig 9). This novel result underlines the versatility of MyoX FERM domain for interacting with different adhesive receptors.

We visualized the synchronous transit of MyoX and VE-Cad to or from the tips of filopodia. The forward movement that reflects the barbed end-directed movement of MyoX occurs at an average velocity of  $700 \text{ nm.s}^{-1}$  (Fig 11), a value similar to that reported in the literature (21). This is also consistent with the

$500 \text{ nm.s}^{-1}$  rate of the recombinant MyoX head moving on actin filaments *in vitro* (20). This similitude between *in vivo* and *in vitro* velocities indicates that the rate of MyoX motion is not affected by the transport of cargoes as heavy as the VE-Cad-catenin complex. The backward movement exhibits a mean rate of  $27 \text{ nm.s}^{-1}$  and allows the redistribution of VE-Cad at the cell body membrane. This motion is probably coupled to the continuous actin retrograde flow that causes the net transport of actin molecules within filaments from the plus end at the tip of a filopodium towards the minus end at the cell body. The speed of VE-Cad retrograde movement matches the speed for actin retrograde flow that is approximately  $33 \text{ nm.s}^{-1}$  (32). Moreover, it could be noticed that the forward and backward movements are frequently interrupted by pausing events. They can be interpreted as the detaching of MyoX from actin cables or as the transient harpooning of either MyoX or its VE-Cad cargo by proteins in their close vicinity.

In **Movie 10**, we showed that cells sound their environment by emitting filopodia that propel VE-Cad molecules against neighbouring cells. At these contact sites, VE-Cad elaborates homophilic interactions with VE-Cad partner molecules present in the counter membranes to constitute the first cell-cell anchor points. Subsequently, intercellular bridges between adjoining cells form and additional VE-Cad molecules transit on them prior to be engaged in their turn in homophilic interactions. VE-Cad accumulation thus reinforces the strength of these preliminary contacts.

VE-Cad molecules on their way back to the cell edges may be picked up again by other growing filopodia. These to-and-fro movements may adjust the local concentration of VE-Cad to the cell needs in specific sites where cell-cell contacts are constructed or remodelled. Moreover, blockage of MyoX-mediated transport by a dominant-negative approach prevents the transportation of VE-Cad at the plasma membrane and subsequently, inhibited formation of endothelial cell-cell contacts (Fig 14 A and B).

Once engaged in homophilic interactions, we frequently observed that VE-Cad moved along cortical actin fibers thus assisting the lateral extension of cell-cell contacts (data not shown). At these more mature adhesion cell-

cell contact sites, no co-localization of MyoX and VE-Cad was detected suggesting that this motor protein is an effective partner for VE-Cad within filopodia but not in mature junctions (**Fig 8**). This probably reflects the heterogeneity existing between the actin filaments inserted into filopodia and those decorating cell-cell junctions that form, in endothelial cells, a continuous thin belt (**Fig 5**). This feature is in agreement with the existence of regioselective actin filament populations on which some myosins are recruited and other ones excluded (**10**).

MyoX-mediated accumulation of VE-Cad at filopodium tips is an important event probably involved in the restoration of endothelial monolayer integrity or in reclosure of wounds (**Movie 10**). The multiplicity of cell-cell

contacts created by filopodia that form bridges between adjacent cells seems to participate in the stabilization of nascent cell-cell junctions.

In conclusion, we showed here that MyoX transports VE-Cad, an endothelial specific cadherin to the tips of filopodia to promote homotypic cell-cell junction formation. A major goal for the future will be to examine whether this MyoX-supported transport of VE-Cad participates in the endothelium remodeling *in vivo*, in pathophysiological situations including endothelium repair or angiogenesis. In addition, it will be interesting to determine whether the concept of myosin-mediated transport of cadherins can be extended to tissues expressing other members of the cadherin family.

## ACKNOWLEDGMENTS

We are indebted to the staff of the maternity from Hôpital Nord (Grenoble, France) for kindly collecting umbilical cords. This work was supported by the « Ligue Régionale de Savoie Contre le Cancer », the « Agence Nationale de la Recherche » (ANR, PCV) and the « Association pour la Recherche sur le Cancer » (grants N° 4447 and 3775). S.A. was a recipient of fellowships from the « Commissariat à l’Energie Atomique » (CEA) and the « Agence Nationale de Recherche ». A.C.-P., S. H. and M.D. are recipients of fellowships from the CEA, the « Association de Recherche sur la Polyarthrite » and the « Agence Nationale de Recherche » (ANR-06-PCV), respectively. The optical microscopy - cell imaging plate-form and the Institute Albert Bonniot are acknowledged for granting access to the confocal microscopy facilities, help in image acquisition and analysis. The authors thank R.E. Cheney for GFP-Myoxin-X, R.-M. Mège and R.Y. Tsien for DSRed cDNA constructs and L. Blanchoin for helpful discussions.

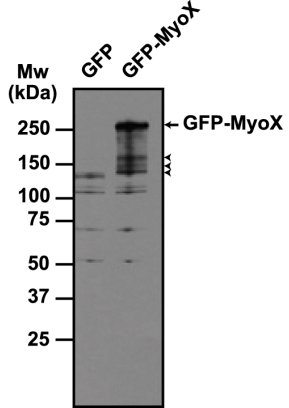
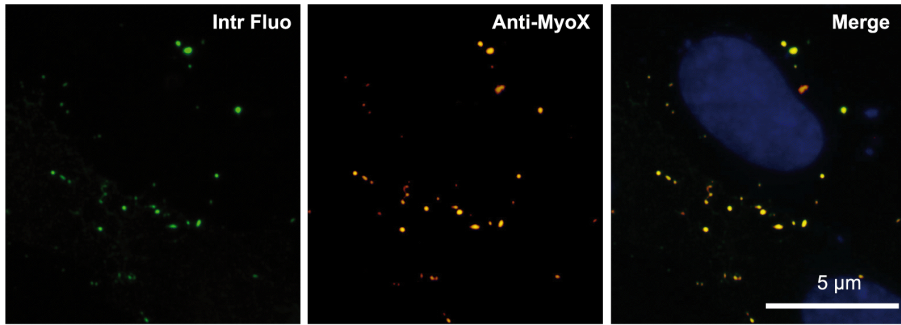
Author contributions: S.A, figures 1, 3, 4 and from 7-15 and all movies; C.D. and S.H., figure 5; A.C.-P., figure 2; O.L. and M.D., figure 6. J.P.S. provided human umbilical cords; P.H. is the head of the laboratory and provided grants, equipments and discussions whereas E.H. helped writing this article; D.G.-D. conceived experiments, interpreted data and wrote the article.

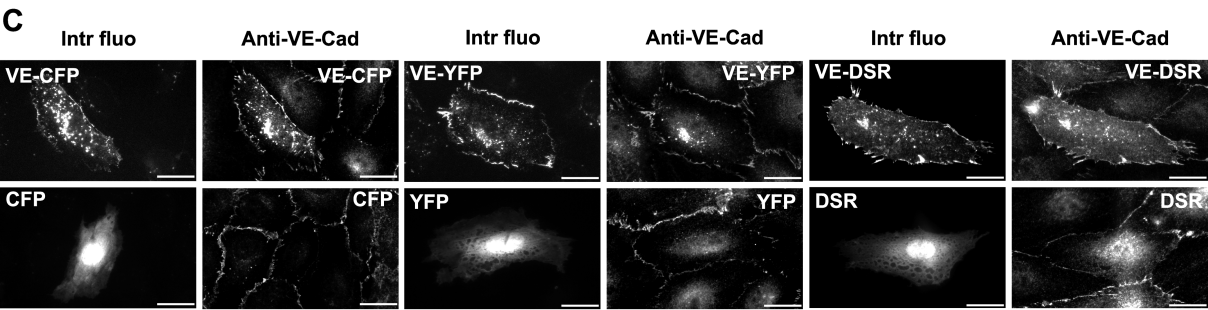
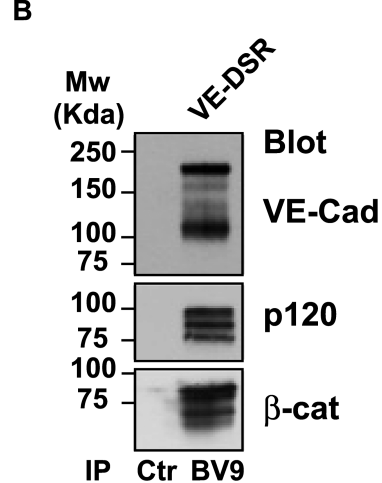
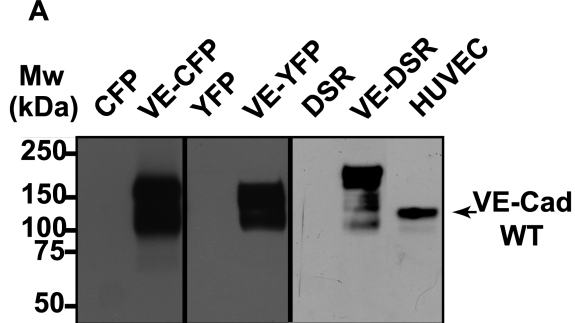
## REFERENCES

1. **Aberle, H., A. Bauer, J. Stappert, A. Kispert, and R. Kemler.** 1997. beta-catenin is a target for the ubiquitin-proteasome pathway. *EMBO J* **16**:3797-804.
2. **Adams, C. L., Y. T. Chen, S. J. Smith, and W. J. Nelson.** 1998. Mechanisms of epithelial cell-cell adhesion and cell compaction revealed by high-resolution tracking of E-cadherin-green fluorescent protein. *J Cell Biol* **142**:1105-19.
3. **Adams, C. L., W. J. Nelson, and S. J. Smith.** 1996. Quantitative analysis of cadherin-catenin-actin reorganization during development of cell-cell adhesion. *J Cell Biol* **135**:1899-911.
4. **Bear, J. E., and F. B. Gertler.** 2009. Ena/VASP: towards resolving a pointed controversy at the barbed end. *J Cell Sci* **122**:1947-53.
5. **Berg, J. S., and R. E. Cheney.** 2002. Myosin-X is an unconventional myosin that undergoes intrafilopodial motility. *Nat Cell Biol* **4**:246-50.
6. **Berg, J. S., B. H. Derfler, C. M. Pennisi, D. P. Corey, and R. E. Cheney.** 2000. Myosin-X, a novel myosin with pleckstrin homology domains, associates with regions of dynamic actin. *J Cell Sci* **113 Pt 19**:3439-51.
7. **Block, J., T. E. Stradal, J. Hanisch, R. Geffers, S. A. Kostler, E. Urban, J. V. Small, K. Rottner, and J. Faix.** 2008. Filopodia formation induced by active mDia2/Drf3. *J Microsc* **231**:506-17.
8. **Bogatcheva, N. V., and A. D. Verin.** 2008. The role of cytoskeleton in the regulation of vascular endothelial barrier function. *Microvasc Res* **76**:202-7.
9. **Bohil, A. B., B. W. Robertson, and R. E. Cheney.** 2006. Myosin-X is a molecular motor that functions in filopodia formation. *Proc Natl Acad Sci U S A* **103**:12411-6.
10. **Brawley, C. M., and R. S. Rock.** 2009. Unconventional myosin traffic in cells reveals a

- selective actin cytoskeleton. *Proc Natl Acad Sci U S A* **106**:9685-90.
11. **Breviario, F., L. Caveda, M. Corada, I. Martin-Padura, P. Navarro, J. Golay, M. Introna, D. Gulino, M. G. Lampugnani, and E. Dejana.** 1995. Functional properties of human vascular endothelial cadherin (7B4/cadherin-5), an endothelium-specific cadherin. *Arterioscler Thromb Vasc Biol* **15**:1229-39.
  12. **Campbell, R. E., O. Tour, A. E. Palmer, P. A. Steinbach, G. S. Baird, D. A. Zacharias, and R. Y. Tsien.** 2002. A monomeric red fluorescent protein. *Proc Natl Acad Sci U S A* **99**:7877-82.
  13. **Coue, M., S. L. Brenner, I. Spector, and E. D. Korn.** 1987. Inhibition of actin polymerization by latrunculin A. *FEBS Lett* **213**:316-8.
  14. **Erdbruegger, U., M. Haubitz, and A. Woywodt.** 2006. Circulating endothelial cells: a novel marker of endothelial damage. *Clin Chim Acta* **373**:17-26.
  15. **Faix, J., D. Breitsprecher, T. E. Stradal, and K. Rottner.** 2009. Filopodia: Complex models for simple rods. *Int J Biochem Cell Biol* **41**:1656-64.
  16. **Gulino, D., E. Delachanal, E. Concord, Y. Genoux, B. Morand, M. O. Valiron, E. Sulpice, R. Scaife, M. Alemany, and T. Vernet.** 1998. Alteration of endothelial cell monolayer integrity triggers resynthesis of vascular endothelium cadherin. *J Biol Chem* **273**:29786-93.
  17. **Gupton, S. L., and F. B. Gertler.** 2007. Filopodia: the fingers that do the walking. *Sci STKE* **2007**:re5.
  18. **Hermant, B., S. Bibert, E. Concord, B. Dublet, M. Weidenhaupt, T. Vernet, and D. Gulino-Debrac.** 2003. Identification of proteases involved in the proteolysis of vascular endothelium cadherin during neutrophil transmigration. *J Biol Chem* **278**:14002-12.
  19. **Heyraud, S., M. Jaquinod, C. Durmort, E. Dambroise, E. Concord, J. P. Schaal, P. Huber, and D. Gulino-Debrac.** 2008. Contribution of annexin 2 to the architecture of mature endothelial adherens junctions. *Mol Cell Biol* **28**:1657-68.
  20. **Homma, K., J. Saito, R. Ikebe, and M. Ikebe.** 2001. Motor function and regulation of myosin X. *J Biol Chem* **276**:34348-54.
  21. **Kerber, M. L., D. T. Jacobs, L. Campagnola, B. D. Dunn, T. Yin, A. D. Sousa, O. A. Quintero, and R. E. Cheney.** 2009. A Novel Form of Motility in Filopodia Revealed by Imaging Myosin-X at the Single-Molecule Level. *Curr Biol*.
  22. **Lampugnani, M. G., M. Resnati, M. Raiteri, R. Pigott, A. Pisacane, G. Houen, L. P. Ruco, and E. Dejana.** 1992. A novel endothelial-specific membrane protein is a marker of cell-cell contacts. *J Cell Biol* **118**:1511-22.
  23. **Maddugoda, M. P., M. S. Crampton, A. M. Shewan, and A. S. Yap.** 2007. Myosin VI and vinculin cooperate during the morphogenesis of cadherin cell cell contacts in mammalian epithelial cells. *J Cell Biol* **178**:529-40.
  24. **Mallavarapu, A., and T. Mitchison.** 1999. Regulated actin cytoskeleton assembly at filopodium tips controls their extension and retraction. *J Cell Biol* **146**:1097-106.
  25. **Martel, V., L. Vignoud, S. Dupe, P. Frchet, M. R. Block, and C. Albiges-Rizo.** 2000. Talin controls the exit of the integrin alpha 5 beta 1 from an early compartment of the secretory pathway. *J Cell Sci* **113 ( Pt 11)**:1951-61.
  26. **Mattila, P. K., and P. Lappalainen.** 2008. Filopodia: molecular architecture and cellular functions. *Nat Rev Mol Cell Biol* **9**:446-54.
  27. **Mege, R. M., J. Gavard, and M. Lambert.** 2006. Regulation of cell-cell junctions by the cytoskeleton. *Curr Opin Cell Biol* **18**:541-8.
  28. **Pi, X., R. Ren, R. Kelley, C. Zhang, M. Moser, A. B. Bohil, M. Divito, R. E. Cheney, and C. Patterson.** 2007. Sequential roles for myosin-X in BMP6-dependent filopodial extension, migration, and activation of BMP receptors. *J Cell Biol* **179**:1569-82.
  29. **Pollard, T. D.** 2007. Regulation of actin filament assembly by Arp2/3 complex and formins. *Annu Rev Biophys Biomol Struct* **36**:451-77.
  30. **Raich, W. B., C. Agbunag, and J. Hardin.** 1999. Rapid epithelial-sheet sealing in the *Caenorhabditis elegans* embryo requires cadherin-dependent filopodial priming. *Curr Biol* **9**:1139-46.
  31. **Rudini, N., and E. Dejana.** 2008. Adherens junctions. *Curr Biol* **18**:R1080-2.
  32. **Schelhaas, M., H. Ewers, M. L. Rajamaki, P. M. Day, J. T. Schiller, and A. Helenius.** 2008. Human papillomavirus type 16 entry: retrograde cell surface transport along actin-rich protrusions. *PLoS Pathog* **4**:e1000148.
  33. **Sousa, A. D., J. S. Berg, B. W. Robertson, R. B. Meeker, and R. E. Cheney.** 2006. Myo10 in brain: developmental regulation, identification of a headless isoform and dynamics in neurons. *J Cell Sci* **119**:184-94.
  34. **Svitkina, T. M., E. A. Bulanova, O. Y. Chaga, D. M. Vignjevic, S. Kojima, J. M. Vasiliev, and G. G. Borisy.** 2003. Mechanism of filopodia initiation by reorganization of a dendritic network. *J Cell Biol* **160**:409-21.
  35. **Tesfamariam, B., and A. F. DeFelice.** 2007. Endothelial injury in the initiation and

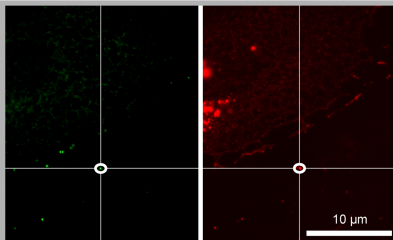
- progression of vascular disorders. *Vascul Pharmacol* **46**:229-37.
36. **Tokuo, H., and M. Ikebe.** 2004. Myosin X transports Mena/VASP to the tip of filopodia. *Biochem Biophys Res Commun* **319**:214-20.
37. **Tokuo, H., K. Mabuchi, and M. Ikebe.** 2007. The motor activity of myosin-X promotes actin fiber convergence at the cell periphery to initiate filopodia formation. *J Cell Biol* **179**:229-38.
38. **Vasioukhin, V., C. Bauer, M. Yin, and E. Fuchs.** 2000. Directed actin polymerization is the driving force for epithelial cell-cell adhesion. *Cell* **100**:209-19.
39. **Vasioukhin, V., and E. Fuchs.** 2001. Actin dynamics and cell-cell adhesion in epithelia. *Curr Opin Cell Biol* **13**:76-84.
40. **Wallez, Y., F. Cand, F. Cruzalegui, C. Wernstedt, S. Souchelnytskyi, I. Vilgrain, and P. Huber.** 2007. Src kinase phosphorylates vascular endothelial-cadherin in response to vascular endothelial growth factor: identification of tyrosine 685 as the unique target site. *Oncogene* **26**:1067-77.
41. **Waschke, J., F. E. Curry, R. H. Adamson, and D. Drenckhahn.** 2005. Regulation of actin dynamics is critical for endothelial barrier functions. *Am J Physiol Heart Circ Physiol* **288**:H1296-305.
42. **Wood, W., and P. Martin.** 2002. Structures in focus--filopodia. *Int J Biochem Cell Biol* **34**:726-30.
43. **Zhang, H., J. S. Berg, Z. Li, Y. Wang, P. Lang, A. D. Sousa, A. Bhaskar, R. E. Cheney, and S. Stromblad.** 2004. Myosin-X provides a motor-based link between integrins and the cytoskeleton. *Nat Cell Biol* **6**:523-31.

**A****B**



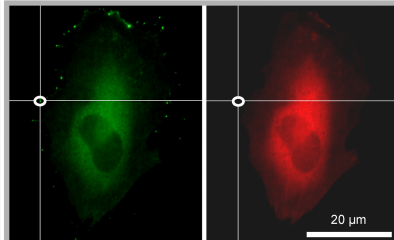
**GFP-MyoX**

**VE-DSR**



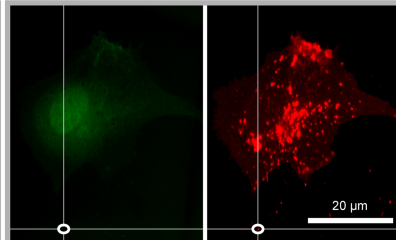
**GFP-MyoX**

**DSR**



**GFP**

**VE-DSR**



3.08  $\mu\text{m}$

6.64  $\mu\text{m}$

A

B

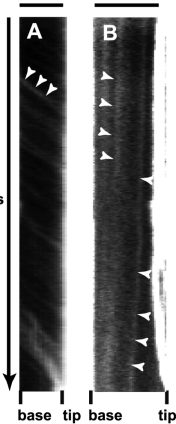
53 s

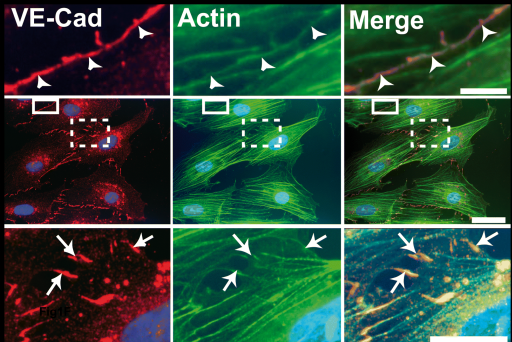
base

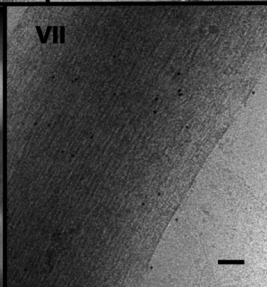
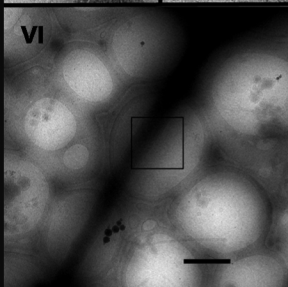
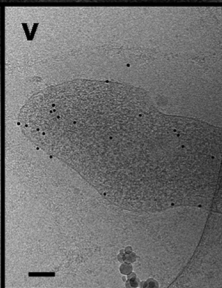
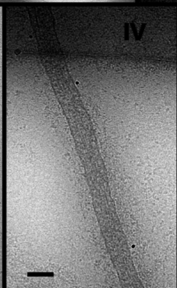
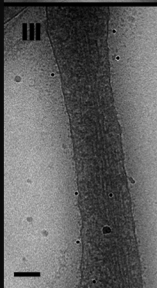
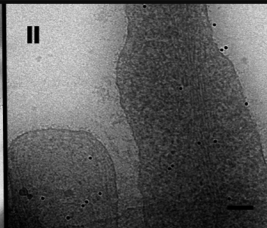
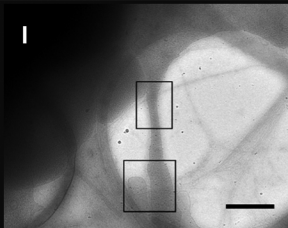
tip

base

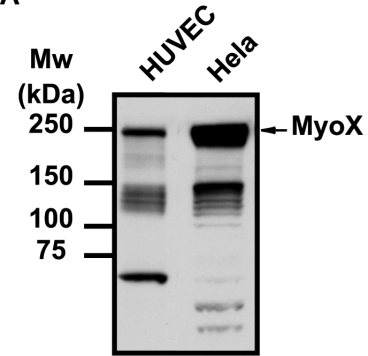
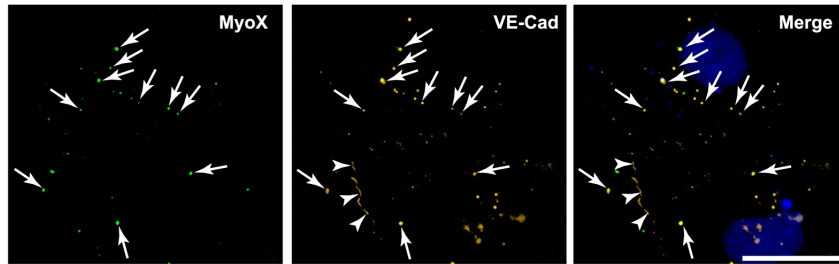
tip

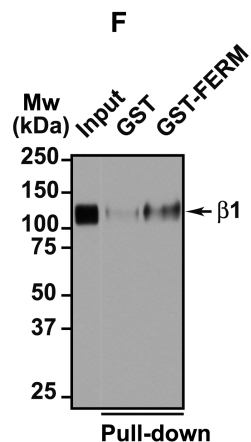
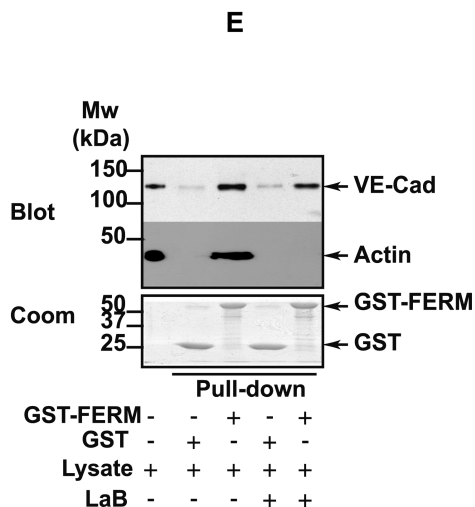
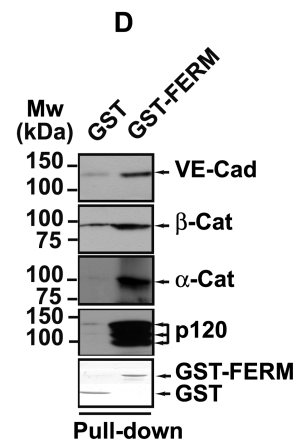
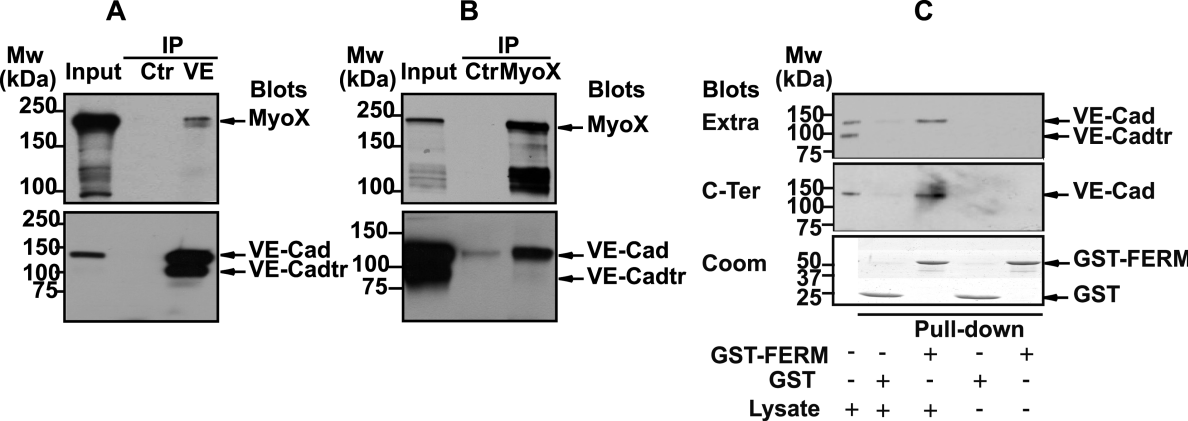


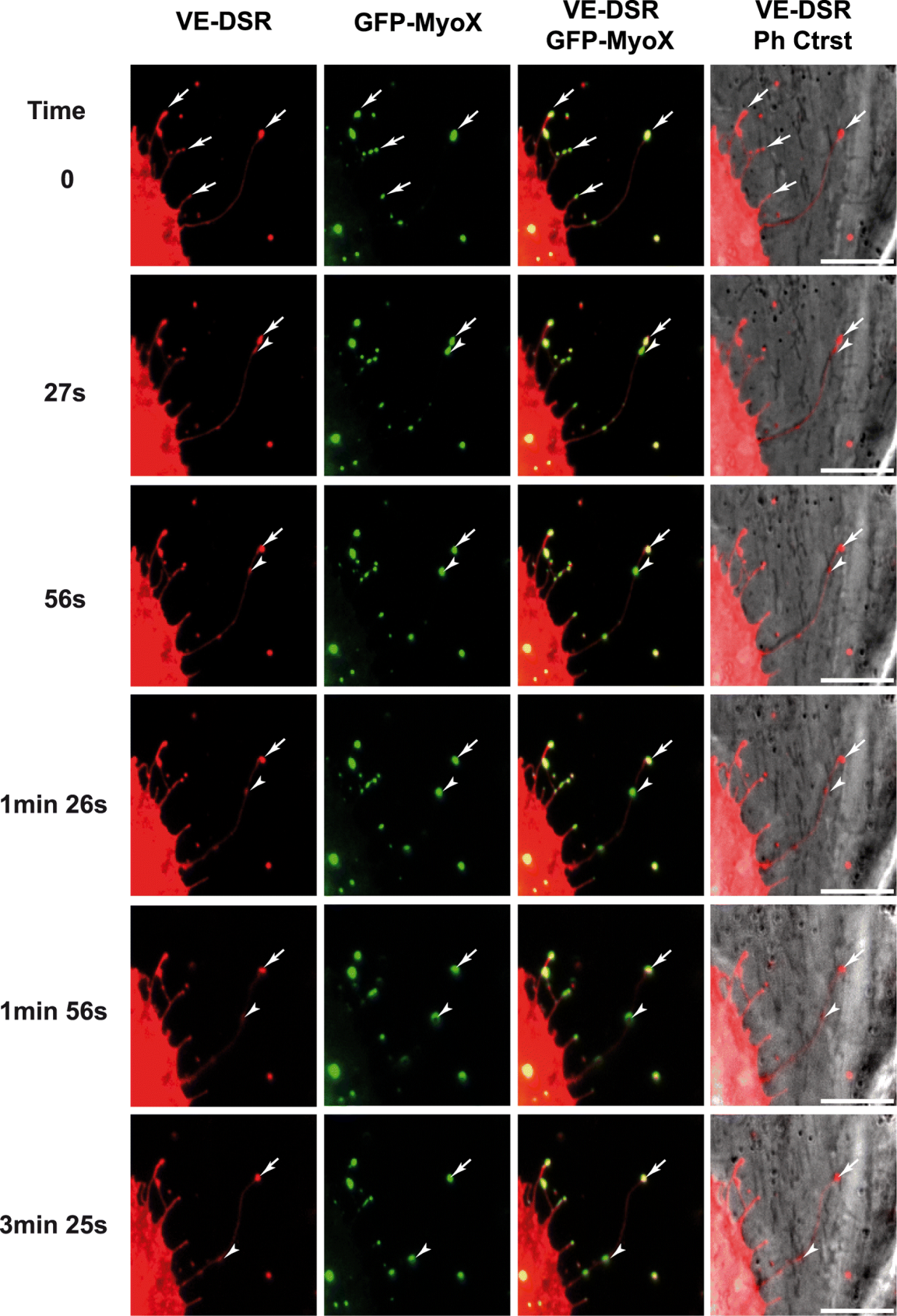


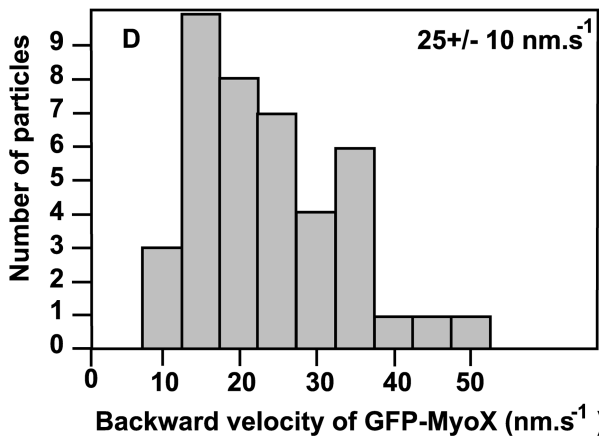
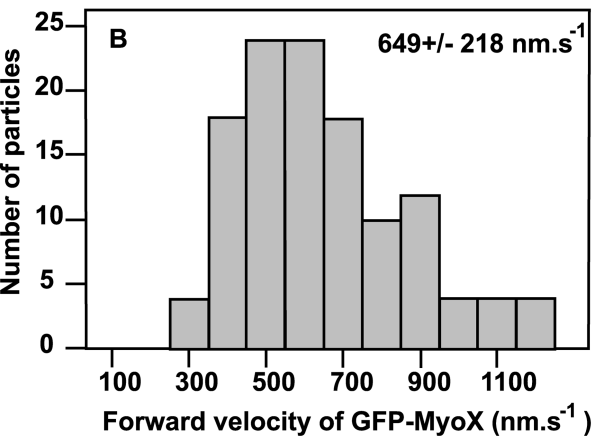
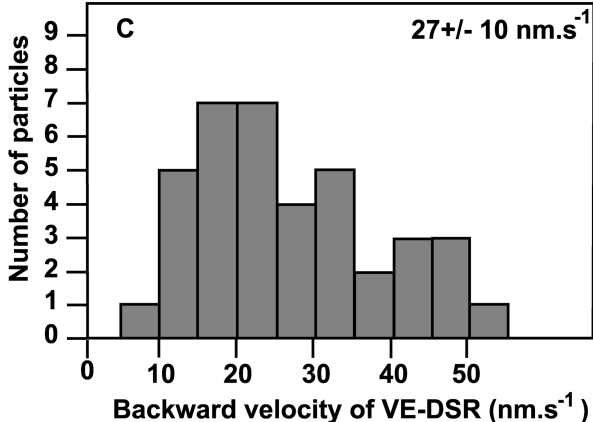
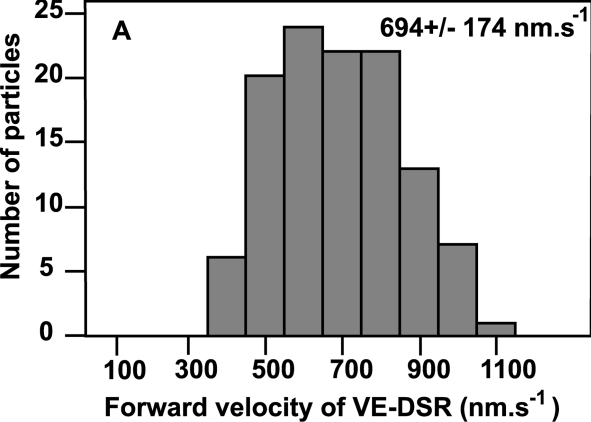




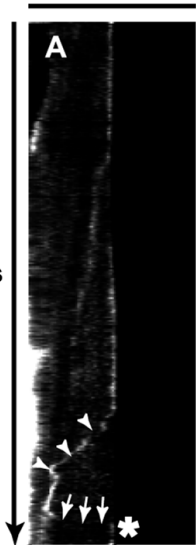
**A****B**







8.10  $\mu\text{m}$

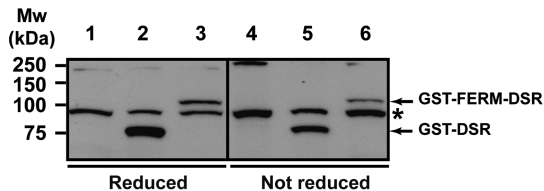


8.10  $\mu\text{m}$

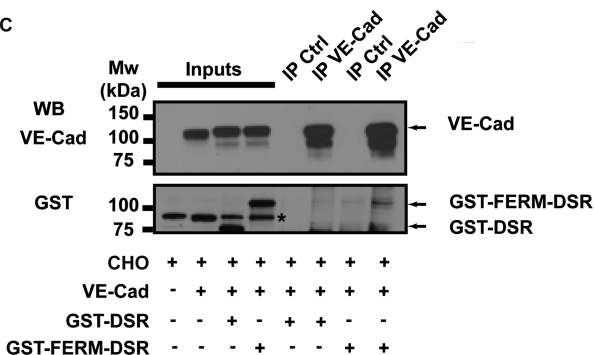




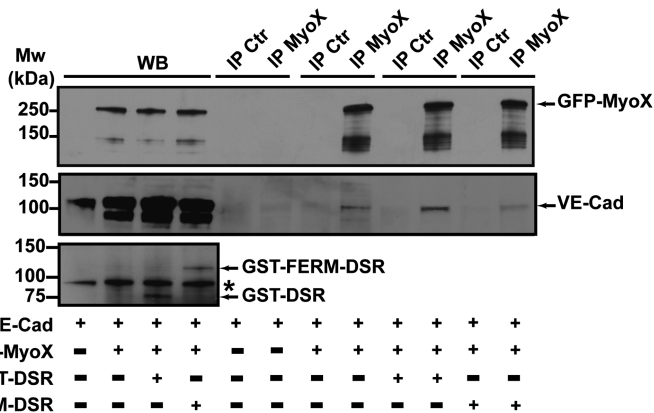
B

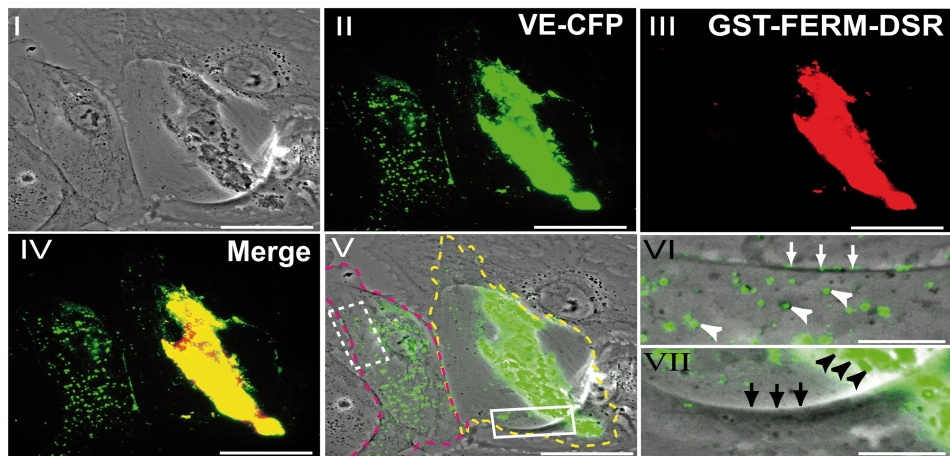


C



D



**A****B****Ctrl****GST-FERM-DSR**

Time (min)

